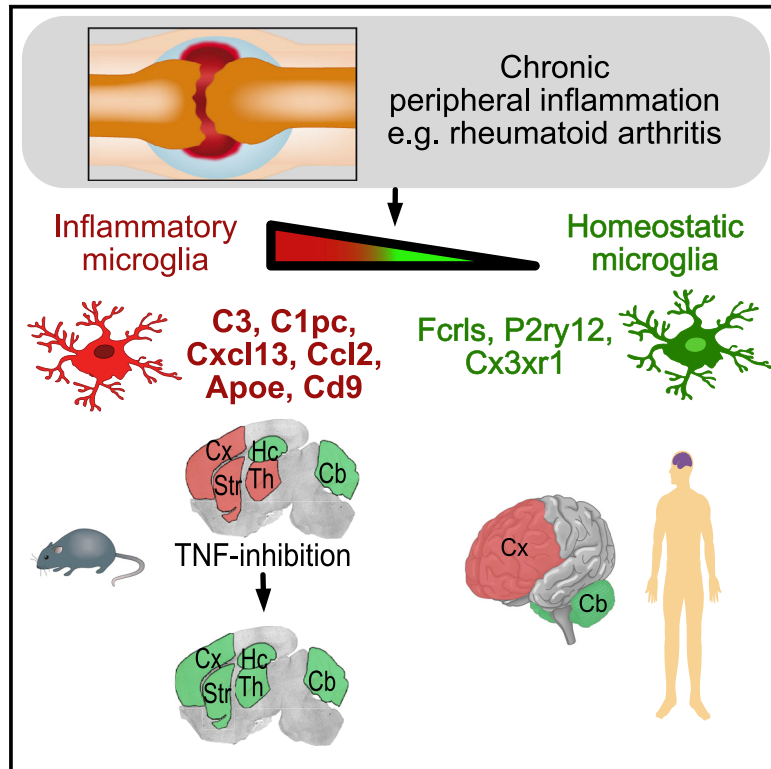


# Cell Reports

## Chronic Peripheral Inflammation Causes a Region-Specific Myeloid Response in the Central Nervous System

### Graphical Abstract



### Authors

Patrick Süß, Alana Hoffmann, Tobias Rothe, ..., Christopher K. Glass, Jürgen Winkler, Johannes C.M. Schlachetzki

### Correspondence

jschlachetzki@health.ucsd.edu

### In Brief

Süß et al. find that chronic peripheral inflammation in mice affects microglia in a brain-region-specific manner, which is reversible upon treatment with a TNF- $\alpha$  inhibitor. Analysis of postmortem tissue suggests a similar spatial pattern of myeloid cell response in patients with rheumatoid arthritis.

### Highlights

- Chronic peripheral inflammation induces microglia activation in the brain
- The microglia response is confined to distinct anatomical brain regions
- Microglia activation is reversible by immunotherapy in the periphery



# Chronic Peripheral Inflammation Causes a Region-Specific Myeloid Response in the Central Nervous System

Patrick Süß,<sup>1,2,8</sup> Alana Hoffmann,<sup>1,8</sup> Tobias Rothe,<sup>3,4,8</sup> Zhengyu Ouyang,<sup>5</sup> Wolfgang Baum,<sup>3</sup> Ori Staszewski,<sup>2</sup> Georg Schett,<sup>3,4</sup> Marco Prinz,<sup>2,6,7</sup> Gerhard Krönke,<sup>3,4</sup> Christopher K. Glass,<sup>5</sup> Jürgen Winkler,<sup>1</sup> and Johannes C.M. Schlachetzki<sup>1,5,9,\*</sup>

<sup>1</sup>Department of Molecular Neurology, Friedrich Alexander University Erlangen-Nürnberg, University Hospital Erlangen, 91054 Erlangen, Germany

<sup>2</sup>Institute of Neuropathology, Faculty of Medicine, University of Freiburg, 79106 Freiburg im Breisgau, Germany

<sup>3</sup>Department of Internal Medicine 3, Friedrich Alexander University Erlangen-Nürnberg, University Hospital Erlangen, 91054 Erlangen, Germany

<sup>4</sup>Deutsches Zentrum für Immuntherapie, 91054 Erlangen, Germany

<sup>5</sup>Department of Cellular and Molecular Medicine, University of California, San Diego, La Jolla, CA 92093, USA

<sup>6</sup>Signalling Research Centres for BIOS and CIBSS, University of Freiburg, 79104 Freiburg im Breisgau, Germany

<sup>7</sup>Center for Basics in NeuroModulation (NeuroModulBasics), Faculty of Medicine, University of Freiburg, 79104 Freiburg im Breisgau, Germany

<sup>8</sup>These authors contributed equally

<sup>9</sup>Lead Contact

\*Correspondence: [jschlachetzki@health.ucsd.edu](mailto:jschlachetzki@health.ucsd.edu)

<https://doi.org/10.1016/j.celrep.2020.02.109>

## SUMMARY

Systemic immune dysregulation contributes to the development of neuropsychiatric and neurodegenerative diseases. The precise effect of chronic peripheral immune stimulation on myeloid cells across anatomical brain regions is unclear. Here, we demonstrate brain-region-specific differences in myeloid responses induced by chronic peripheral inflammation. This shift in the myeloid compartment is associated with the appearance of an inflammatory myeloid subpopulation in the cortex, striatum, and thalamus accompanied by regional transcriptomic fingerprints that include induction of chemokines, complement factors, and endothelial adhesion molecules. In contrast, myeloid immune responses within the hippocampus and cerebellum are subtle or absent. Treatment with the anti-tumor necrosis factor  $\alpha$  (anti-TNF- $\alpha$ ) antibody infliximab ablates the region-specific inflammatory response. A region-specific myeloid cell response to chronic peripheral inflammation is observed in postmortem brains from individuals with rheumatoid arthritis. Our data suggest that chronic peripheral inflammation has heterogeneous effects on the brain, as evidenced by the spectrum of myeloid cell responses observed across brain regions.

## INTRODUCTION

Immune activation in the periphery affects the function of the central nervous system (CNS) and is associated with an

increased risk of developing neuropsychiatric and neurodegenerative diseases (Czirr and Wyss-Coray, 2012; Dantzer et al., 2008b). The interplay between the peripheral immune system and the brain is exerted and modulated by CNS myeloid cells, including microglia, perivascular macrophages, as well as infiltrating bone marrow-derived monocytes under pathological conditions (Prinz et al., 2011). Alterations in microglia phenotype mediated by routes involving blood-brain barrier (BBB) endothelial cells, leptomeninges, the choroid plexus, and vagal nerve afferents have been observed in various models of peripheral inflammation (Balusu et al., 2016; Blank et al., 2016; D'Mello and Swain, 2017; Sankowski et al., 2015; Wu et al., 2005). Systemic immune mediators like the cytokine tumor necrosis factor  $\alpha$  (TNF- $\alpha$ ) are connected to the presence of depression, altered pain perception, fatigue, and cognitive impairment, as well as an increased prevalence of Alzheimer's disease (AD) (Capuron and Miller, 2011; Chou et al., 2016; Dantzer et al., 2008a; Uguz et al., 2009). Increased sustained systemic levels of TNF- $\alpha$  and propagation of peripheral inflammation into the CNS has been proposed to play a major role for the development of chronic pain, depression, anxiety, and dementia in later life in individuals with rheumatoid arthritis (RA), a chronic inflammatory disease characterized by synovial inflammation and bone erosions (McInnes and Schett, 2011; Nerurkar et al., 2019; Wallin et al., 2012).

The effect of the peripheral immune system on the brain, and microglia in particular, has been predominantly studied in the context of an acute stimulus, mainly mimicking sepsis through injection of the gram-negative endotoxin lipopolysaccharide (LPS). Peripheral LPS injections shift microglia into a pro-inflammatory phenotype as demonstrated by changes in the gene expression signature, morphology, and number (Hoogland et al., 2015; Kloss et al., 2001). Repeated acute peripheral stimuli promote immune training and tolerance in the brain by promoting



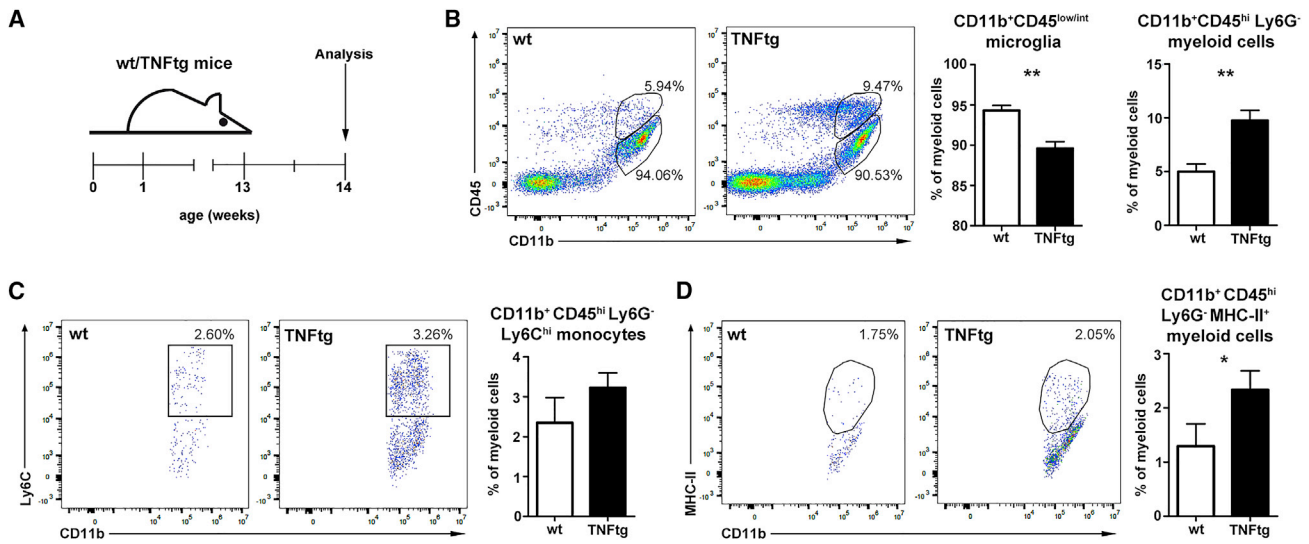


**Figure 1. Flow Cytometry of CNS Myeloid Cells in WT and TNFtg Mice**

(A) Experimental paradigm depicting the analysis of whole-brain homogenates of WT and TNFtg mice at the age of 14 weeks.

(B) Proportion of CD11b<sup>+</sup>CD45<sup>low/int</sup> microglia in the whole brain.

(C) Fraction of CD11b<sup>+</sup>CD45<sup>hi</sup>Ly6G<sup>-</sup> myeloid cells in the whole brain.

(D) Frequency of CD11b<sup>+</sup>CD45<sup>hi</sup>Ly6G<sup>-</sup>Ly6C<sup>hi</sup> blood-derived monocytes in the brain of WT and TNFtg mice.

(E) Frequency of CD11b<sup>+</sup>CD45<sup>hi</sup>Ly6G<sup>-</sup>MHC-II<sup>+</sup> myeloid cells.

All data represent one of three independent experiments with n = 4 WT and n = 5 TNFtg mice. Data are depicted as means ± SEM. Analysis was performed using unpaired Student's t test (\*p < 0.05; \*\*p < 0.01).

long-term enhancer activation in microglia (Wendeln et al., 2018). However, whether a chronic systemic inflammatory challenge promotes similar effects on the brain innate immune system is vastly unknown.

While most studies addressing the impact of peripheral inflammation on the CNS did not distinguish between distinct brain regions, there is emerging evidence that immune responses in the brain are regulated in a site-specific manner. Regional differences have been reported in phagocytic capacity, marker expression, and transcriptomic subcluster distribution of murine and human microglia (Ayata et al., 2018; Böttcher et al., 2019; Grabert et al., 2016; Hammond et al., 2019; Masuda et al., 2019). After LPS injection, regional increases in microglia density have been reported (Furube et al., 2018; Kim et al., 2000).

We hypothesized that chronic systemic peripheral inflammation induces a CNS myeloid cell response being restricted to distinct anatomical brain regions. We used the human TNF- $\alpha$  transgenic mouse model of RA (TNFtg mice, strain Tg197) (Keffer et al., 1991), which shows increased levels of peripheral cytokines and severe joint pathology at young age leading to severe disability within 3–4 months after birth (Keffer et al., 1991). We detected region-specific alterations in the CNS myeloid cell composition associated with a distinct gene expression profile. Interestingly, treatment with the anti-TNF- $\alpha$  antibody infliximab (IFX) led to a reversal of the regional inflammatory profile in the mouse brain. These findings were complemented by analysis of postmortem samples from RA patients indicating altered microglia phenotypes confined to the cortex, but not the cerebellum. Our data demonstrate that immune changes in the periphery lead to alterations in myeloid cell phenotypes in the

CNS in a region-dependent manner. Further understanding of the different brain microenvironments and their susceptibility to an immune challenge may lead to greater insight in the contribution of myeloid cells to the pathogenesis of neurodegenerative and neuropsychiatric diseases.

## RESULTS

### Increase of Activated Myeloid Cells in the Brain of TNFtg Mice

We previously showed that hippocampal immune state, function, and neurogenesis are resilient to chronic peripheral inflammation in TNFtg mice (Süß et al., 2015). Therefore, we asked whether other brain regions of TNFtg mice, which show an increase in peripheral immune activation from 4 weeks onward, exhibit any changes in the composition of myeloid cells (Keffer et al., 1991). To address this question, we first performed flow cytometry analysis of whole-brain homogenates from 14-week-old wild-type (WT) and TNFtg mice (Figure 1A). Cells were gated on CD11b and CD45 to separate CD11b<sup>+</sup>CD45<sup>low/int</sup> resting microglia from CD11b<sup>+</sup>CD45<sup>hi</sup>Ly6G<sup>-</sup> myeloid cells (Figure S1). We detected a decreased proportion of CD11b<sup>+</sup>CD45<sup>low/int</sup> microglia in TNFtg mice compared to WT (Figure 1B). In contrast, the percentage of CD11b<sup>+</sup>CD45<sup>hi</sup>Ly6G<sup>-</sup> CNS myeloid cells was significantly increased in the brains of TNFtg mice (Figure 1B). CD11b<sup>+</sup>CD45<sup>hi</sup>Ly6G<sup>-</sup> CNS myeloid cells comprise infiltrating monocyte-derived cells, activated microglia, and perivascular macrophages (Goldmann et al., 2016; Ponomarev et al., 2011; Prinz et al., 2011). To deconvolute this heterogeneous cell subpopulation, we analyzed the proportion

of infiltrating Ly6C<sup>hi</sup> inflammatory monocyte-derived cells and the expression of major histocompatibility complex (MHC) class II in the CD11b<sup>+</sup>CD45<sup>hi</sup>Ly6G<sup>-</sup> population (Figure S1). We observed a slight, but nonsignificant increase in the ratio of CD11b<sup>+</sup>CD45<sup>hi</sup>Ly6G<sup>-</sup>Ly6C<sup>hi</sup> inflammatory monocyte-derived cells infiltrating the brain of TNFtg mice (Figure 1C). Moreover, there was a pronounced increase in the percentage of activated CD11b<sup>+</sup>CD45<sup>hi</sup>Ly6G<sup>-</sup>MHC-II<sup>+</sup> myeloid cells (Figure 1D). Taken together, these findings indicate a shift of the brain myeloid cell population to an activated state in the brains of TNFtg mice.

### Region-Specific Myeloid Cell Response in the Brain of TNFtg Mice

To topographically map the myeloid cells detected in flow cytometry to distinct brain regions, we performed immunohistochemistry. We observed a ~1.6-fold increase of parenchymal Iba1<sup>+</sup> cells in the cortex and striatum and a ~2.3-fold increase in the thalamus (Figure 2A). In contrast, the density of Iba1<sup>+</sup> cells was not different in the cerebellum, whereas we observed a slight ~1.2-fold increase in the hippocampus of TNFtg mice compared to WT mice (Figure 2A). To determine the activation state of myeloid cells in different brain regions of TNFtg mice, we co-stained brain sections for Iba1 and CD45 or CD169. We confirmed that CD45 and CD169 are almost exclusively expressed by Iba1<sup>+</sup> myeloid cells and are absent in NeuN<sup>+</sup> neurons, GFAP<sup>+</sup> astrocytes, and Olig2<sup>+</sup> oligodendrocytes (Figure S2). Both markers were previously used to distinguish microglia from inflammatory monocyte-derived cells infiltrating the CNS (Gao et al., 2015; Prinz et al., 2011). However, both CD45 and CD169 are expressed by leptomeningeal, perivascular macrophages, and activated microglia (Fourgeaud et al., 2016; Gosselet et al., 2014; Kierdorf et al., 2019; Perry et al., 1992). We therefore focused on ramified parenchymal cells likely representing microglia and excluded the meninges and perivascular space. Intriguingly, we observed a high density of Iba1<sup>+</sup>/CD45<sup>+</sup> and Iba1<sup>+</sup>/CD169<sup>+</sup> cells in the cortex, striatum, and thalamus of TNFtg mice (Figures 2B and 2C). In contrast, there were no differences in the density of Iba1<sup>+</sup>/CD45<sup>+</sup> and Iba1<sup>+</sup>/CD169<sup>+</sup> cells in the hippocampus and cerebellum between both groups (Figures 2B and 2C). In line with cortical myeloid cell activation, we detected a decreased ratio of homeostatic CD11b<sup>+</sup>CD45<sup>low/int</sup> microglia and increases in CD11b<sup>+</sup>CD45<sup>hi</sup>Ly6G<sup>-</sup> and CD11b<sup>+</sup>CD45<sup>hi</sup>Ly6G<sup>-</sup>MHC-II<sup>+</sup> myeloid cells in the dissected cortex of TNFtg mice by flow cytometry (Figure 2D). Taken together, these findings indicate regional myeloid cell activation in cortex, striatum, and thalamus but very limited alterations in the hippocampus and cerebellum of TNFtg mice.

### Regional Transcriptional Response to Chronic Peripheral Inflammation in the Brains of TNFtg Mice

Next, we wondered whether the regional CNS myeloid cell response in the brain of TNFtg mice is mirrored on the transcriptional level. We performed RNA sequencing (RNA-seq) of dissected bulk tissue of the cortex, striatum, thalamus, hippocampus, and cerebellum of WT and TNFtg mice. We detected a total of 497 genes differentially expressed by at least 2-fold in the cortex, striatum, and thalamus, most of which were upregulated in TNFtg mice (Figure 3A; Table S2). In contrast, we did

not observe any gene differentially expressed by at least 2-fold in the hippocampus of TNFtg mice, while only 7 genes were differentially expressed in the cerebellum (Figure 3A; Table S2). Comparison of 497 genes differentially expressed in at least one brain region of TNFtg mice revealed a remarkable overlap of 129 genes mutually altered in the cortex, striatum, and thalamus (Figure 3A, S3A, and S3B). Out of those 129 genes, 127 were upregulated in all three regions (Table S2) and only 4 genes were also found differentially expressed in the cerebellum (Figures 3A and S3A). Accordingly, principal-component analysis based on the expression of 497 differentially expressed genes revealed close clustering of the cortex, striatum, and thalamus of TNFtg mice, clearly distant from the remaining brain regions of TNFtg mice and all WT brain regions (Figure 3B). Hierarchical clustering further illustrated a clear separation of the cortex, striatum, and thalamus of TNFtg mice from the respective brain regions of WT mice as well as the cerebella and hippocampi of both experimental groups (Figures 3C and S3C). The cortex, striatum, and thalamus of TNFtg mice further shared many of the most strongly upregulated genes, including the chemokines *Cxcl13* and *Ccl2* and the complement factor genes *C3* and *C4b* (Figure 3D). Having detected a regional gene expression signature in the brain of TNFtg mice, we performed qPCR analysis to validate our findings obtained by RNA-seq. First, we compared the mRNA levels of the chemokines *Cxcl13*, *Ccl8*, and *Ccl2* in different brain regions of WT and TNFtg mice. We observed a similar pattern of regional chemokine induction compared to RNA-seq, with a high increase in the cortex, striatum, and thalamus and a less pronounced nonsignificant tendency in the hippocampus of TNFtg mice compared to the corresponding WT brain region (Figure S4A). Based on the expression analysis of *C3*, *C4b*, and *C1s1*, the complement system was most profoundly induced in the cortex, striatum, and thalamus and showed only minor changes in the cerebellum and hippocampus of TNFtg mice (Figure S4B).

To exclude that the regional transcriptional changes are partially caused by a regional expression of the human TNF- $\alpha$  transgene by resident CNS cells, we mapped the FASTQ files to the human genome build hg38 (Figure S3E). Human TNF- $\alpha$  was absent or lowly expressed (reads per kilobase per million mapped reads [RPKM] <2) in all regions, except for the cortex, which showed low abundance of human TNF- $\alpha$  expression (RPKM <9).

Next, we aimed to infer the functional relevance of regional transcriptional changes in the brain of TNFtg mice and performed Gene Ontology (GO) analyses of the cortex, striatum, and thalamus of TNFtg mice based on all 497 differentially expressed genes. All three regions displayed similar enrichment of GO terms that were almost exclusively assigned to inflammatory response (Figure 3E; Table S3). The most strongly enriched GO terms included leukocyte migration and regulation of cell adhesion, which further supports peripheral immune cell infiltration into the cortex, striatum, and thalamus of TNFtg mice (Figure 3E; Table S3). Moreover, we found myeloid leukocyte activation as a term enriched in the cortex, striatum, and thalamus of TNFtg mice. Interestingly, the cortex, striatum, and thalamus also showed a transcriptional signature linked to RA (Figure 3E; Table S3). When GO analysis was focused on

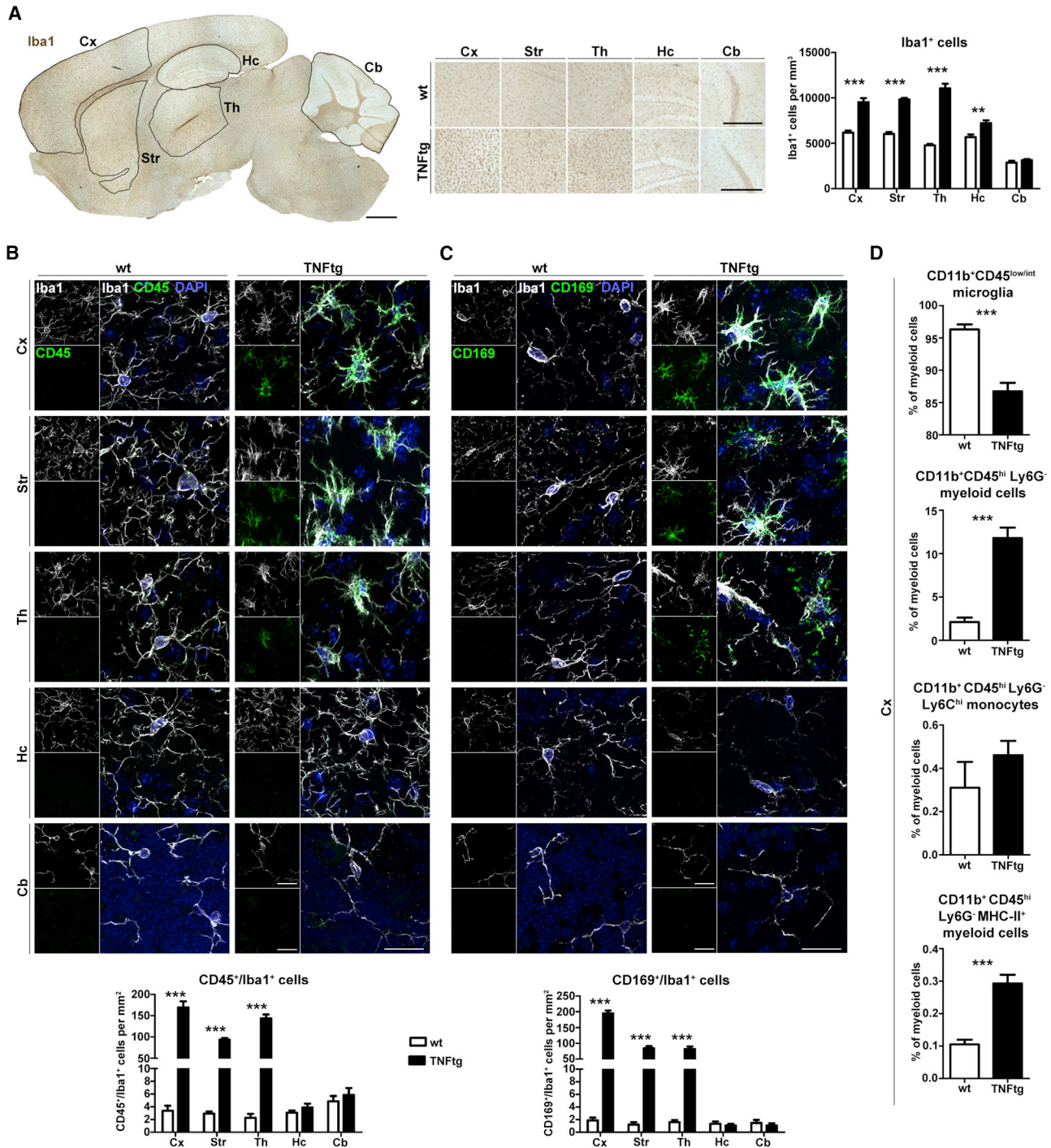


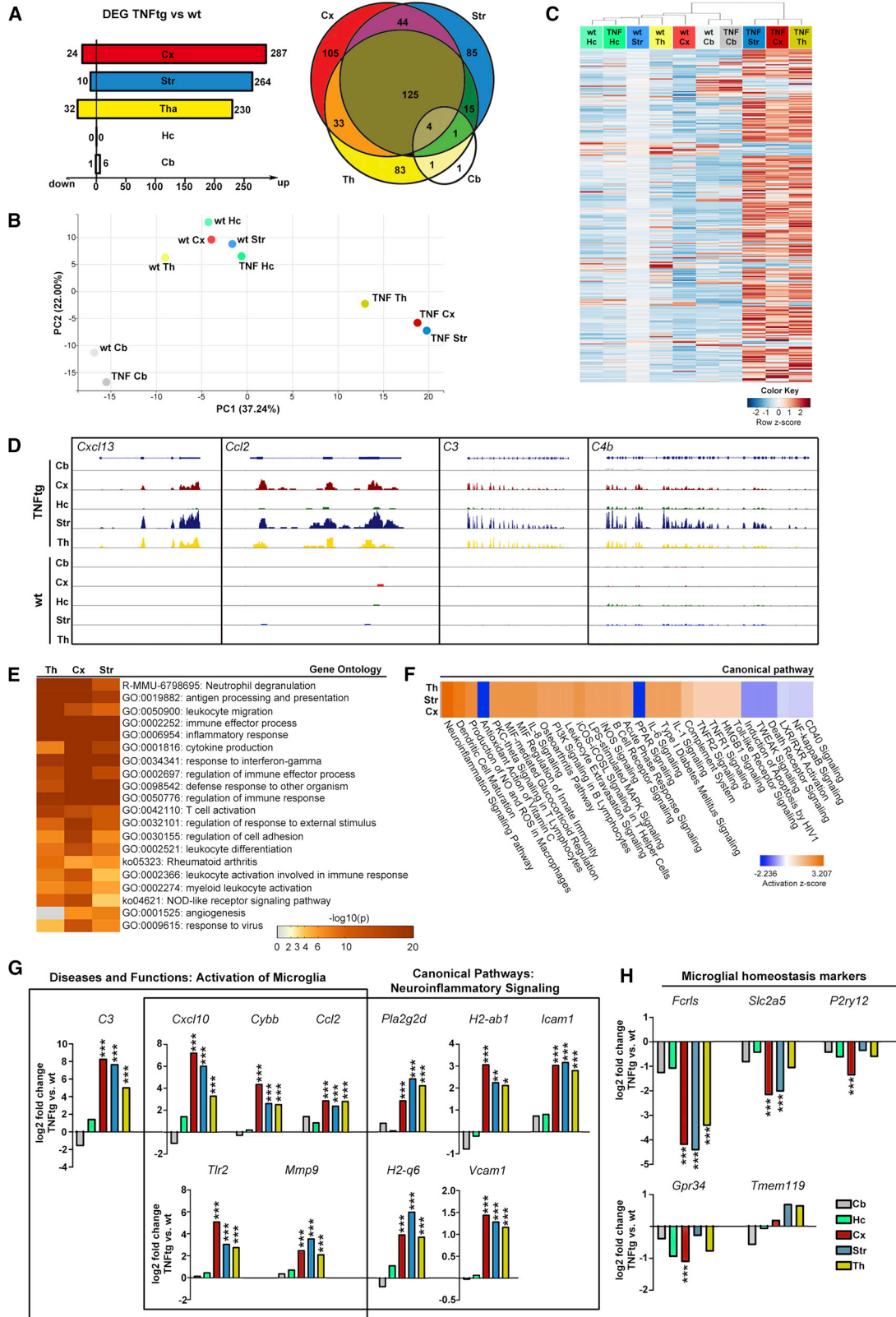
**Figure 2. Regionally Restricted Myeloid Cell Activation in the Brain of TNFtg Mice**

(A) Density of Iba1<sup>+</sup> myeloid cells in the cortex (Cx), striatum (Str), thalamus (Th), hippocampus (Hc), and cerebellum (Cb) of WT (n = 5) and TNFtg mice (n = 6). Analyzed brain regions are delineated. Cortical subregions comprise the frontal pole, the somatomotor cortex, and the somatosensory cortex. Scale bars represent 1,000  $\mu$ m (overview) and 500  $\mu$ m (regional insets).

(B and C) Co-expression of the activation markers CD45 (B) and CD169 (C) in parenchymal myeloid cells in brain regions of WT and TNFtg mice. n = 5 WT and n = 6 TNFtg mice (B); n = 5 per group (C). Scale bars, 10  $\mu$ m.

(D) Flow cytometry of myeloid cells in the dissected cortex of WT and TNFtg mice (n = 4 per group) following the gating strategy shown in Figure S1.

All data are presented as means  $\pm$  SEM. Analysis was performed using two-way ANOVA followed by Bonferroni's post hoc test (A–C) and unpaired Student's t test (D) (\*p < 0.05; \*\*p < 0.01; \*\*\*p < 0.001).



(legend on next page)

the  $n = 127$  genes commonly upregulated in the cortex, striatum, and thalamus of TNFtg mice (Table S3), a similar GO term enrichment linked to inflammatory response was observed (Figure S3D).

To more thoroughly dissect the common signature of the cortex, striatum, and thalamus and compare it to the hippocampus and cerebellum, we performed Ingenuity Pathway Analysis (IPA) based on the 127 regional log<sub>2</sub> fold increased genes commonly upregulated in the cortex, striatum, and thalamus of TNFtg mice. We detected inflammation-associated canonical pathways that were strongly activated in the cortex, striatum, and thalamus. The IPA pathway most profoundly activated in these three brain regions was neuroinflammatory signaling (Figure 3F). Other canonical pathways regionally activated in the brain of TNFtg mice included the production of nitric oxide (NO) and reactive oxygen species (ROS) in macrophages, leukocyte extravasation, and the complement system (Figure 3F). We then focused on the genes assigned to neuroinflammatory signaling. Several of those genes were among the most strongly induced genes in the cortex, striatum, and thalamus of TNFtg mice, including *Cxcl10*, *Pla2g2d*, and MHC class II genes (Figure 3G; Table S4). We further used IPA of diseases and functions to infer the potential physiological relevance of the regional transcriptional fingerprint in the brain of TNFtg mice. We detected activation of microglia as a significant term profoundly activated in the cortex, striatum, and thalamus of TNFtg mice (Figure 3G; Table S4). Further functional terms suggested movement and infiltration of myeloid cells in the cortex, striatum, and thalamus of TNFtg mice (Table S4). We then asked for potential upstream regulators explaining the regionally restricted inflammatory response in the brain of TNFtg mice. Transcriptional signatures in the cortex, striatum, and thalamus were potentially induced by interferon- $\gamma$  and STAT-1 (Table S4). *Znf106* and *Ptger4* were reported to downregulate several neuroinflammatory genes (Joyce et al., 2016; Shi et al., 2010) and were suggested as negatively regulated upstream transcriptional regulators (Table S4).

As we observed signs of regional microglial activation in the brain of TNFtg mice, we asked for the regulation of microglial homeostasis markers, which are downregulated during the activation of microglia (Bennett et al., 2016; Hickman et al., 2013; Keren-Shaul et al., 2017; Krasemann et al., 2017).

Consistently, we found a strong downregulation of *Fcrls* in the cortex, striatum, and thalamus of TNFtg mice (Figure 3H). Additionally, in the striatum of TNFtg mice, *Slc2a5* was decreased, while in the cortex, there was a downregulation of *Slc2a5*, *P2ry12*, and *Gpr34*. *Tmem119* was not differentially expressed in any brain region of TNFtg mice (Figure 3H). Downregulation of microglial homeostasis markers in the cerebellum and hippocampus was minimal and did not reach significance (Figure 3H). To summarize, these results obtained by transcriptomic analyses strongly indicate an inflammatory transcriptional fingerprint in the cortex, striatum, and thalamus of TNFtg mice with only subtle changes in the hippocampus and cerebellum.

### Single-Cell RNA-Seq of Cortical Myeloid Cells of WT and TNFtg Mice

To examine the response of brain myeloid cells to systemic chronic inflammation, we performed single-cell RNA-seq on isolated CD11b<sup>+</sup>CD45<sup>+</sup> cells from the cortex of WT and TNFtg mice (Figure 4A). After quality control, we obtained single-cell gene expression profiles from 5,543 cells. We obtained five transcriptionally distinct cell subpopulation clusters and annotated the major cell types using SingleR (Figures 4B and S5). The majority of cells were identified as microglia; however, we also identified a cell population of inflammatory macrophages showing markers reminiscent of activated microglia, as discussed below. In addition, we annotated a small number of monocytes ( $n = 135$ ) and granulocytes ( $n = 143$ ). Next, we compared CD11b<sup>+</sup>CD45<sup>+</sup> cells from TNFtg versus WT cortex (Figures 4C and 4D). The proportions of microglia were similar between TNFtg and WT (Figure 4E). However, the cortices of TNFtg mice showed an increased proportion of inflammatory macrophages, whereas the number of monocytes and granulocytes were lower compared to WT.

We next compared if there are qualitative gene expression perturbations in microglia and in cluster 2 (inflammatory macrophages) of TNFtg compared to WT cortices (Figures 4F and S5; Table S5). TNFtg microglia and cluster 2 or inflammatory macrophages demonstrated reductions of various microglia homeostatic genes, including *Fcrls*, *Cx3cr1*, *Tmem119*, and *P2ry12*. Other markers that were upregulated in cluster 2 or inflammatory macrophages and to some extent in TNFtg microglia were *ApoE*,

### Figure 3. Regional Inflammatory Gene Expression in the Brain of TNFtg Mice Revealed by Bulk RNA-Seq

(A) Numbers of differentially expressed genes (fold change >2, adjusted p value <0.05) in the cortex (Cx), striatum (Str), thalamus (Th), hippocampus (Hc), and cerebellum (Cb) of TNFtg mice compared to WT mice. Venn diagram shows the regional overlap of differentially expressed genes.

(B and C) Principal-component analysis (B) and heatmap (C) showing hierarchical clustering of all groups based on  $n = 497$  genes differentially expressed in brain regions of TNFtg mice compared to WT mice.

(D) Representative UCSC Genome Browser tracks displaying normalized profiles of *Cxcl13*, *Ccl2*, *C3*, and *C4b* reads.

(E) Heatmap indicating the most significantly enriched GO terms in the cortex, striatum, and thalamus of TNFtg mice.

(F) Heatmap indicating the most significantly induced canonical pathways in the cortex, striatum, and thalamus of TNFtg mice based on Ingenuity Pathway Analysis (IPA) of  $n = 127$  genes commonly upregulated in the cortex, striatum, and thalamus.

(G) Regional log<sub>2</sub> fold changes of genes representing members of the IPA Canonical Pathway “Neuroinflammation Signaling Pathway” (Table S4) and the IPA Diseases and Functions term “Activation of Microglia” (Table S4) in the cortex, striatum, thalamus, hippocampus, and cerebellum.

(H) Regional expression of microglial homeostatic markers in the cortex, striatum, and thalamus of TNFtg mice. Data are representative of  $n = 4$  WT and TNFtg mice. Prior to sequencing, the striatum, thalamus, and cerebellum of  $n = 1$  as well as the cortex of  $n = 2$  TNFtg mice had to be excluded due to technical reasons. Analysis of differential gene expression was performed using edgeR. Genes with an adjusted p value (p adj.) < 0.05 and a log<sub>2</sub> fold change > 1 between TNFtg and WT mice were considered significantly differentially expressed, \*log<sub>2</sub> fold change > 1 and p adj. < 0.05, \*\*log<sub>2</sub> fold change > 1 and p adj. < 0.01, \*\*\*log<sub>2</sub> fold change > 1 and p adj. < 0.001.

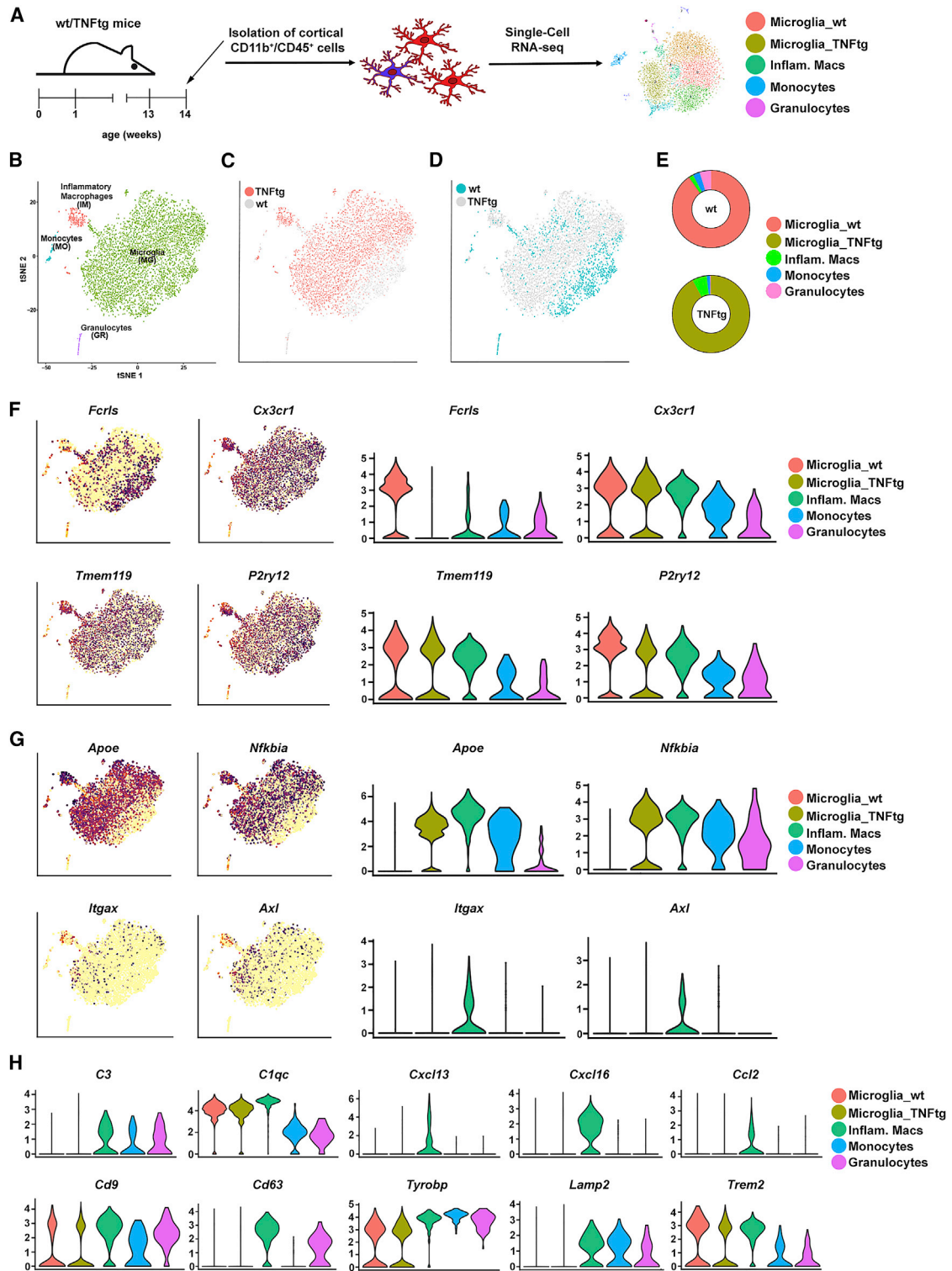


**Figure 4. Single-Cell RNA Sequencing of Live CD11b<sup>+</sup>CD45<sup>+</sup> Myeloid Cells Isolated from the Cortex of WT and TNFtg Mice**

(A) Experimental design.

(B) t-SNE plot showing clustering of 5,543 cortical CD11b<sup>+</sup>CD45<sup>+</sup> myeloid cells from WT (n = 1,326) and TNFtg (n = 4,217) into five subpopulations.

(C) t-SNE plot highlighting cortical CD11b<sup>+</sup>CD45<sup>+</sup> myeloid cells from TNFtg mice.

(D) t-SNE plot showing WT cortical CD11b<sup>+</sup>CD45<sup>+</sup> myeloid cells.

(legend continued on next page)

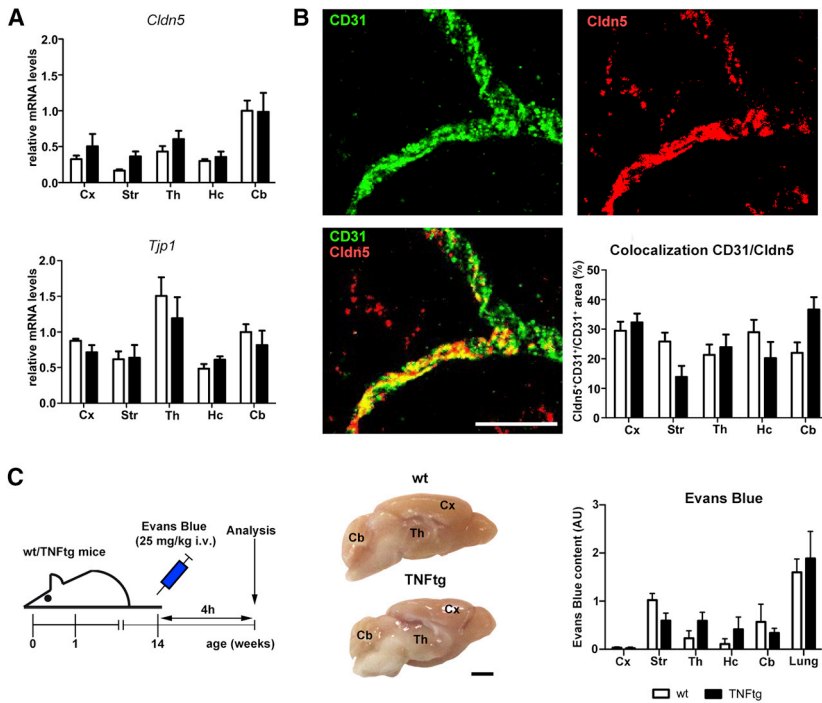


**Figure 5. Global Blood-Brain Barrier (BBB) Integrity in TNFtg Mice**

(A) Regional expression of genes encoding BBB tight junction composites in WT and TNFtg mice (n = 4 per group).

(B) Confocal colocalization analysis of the blood vessel marker CD31 and the tight junction marker claudin 5 (Cldn5) in different brain regions of WT (n = 5) and TNFtg mice (n = 6). Scale bar, 10  $\mu$ m.

(C) Permeation of intravenously injected Evans blue dye through the regional BBB (n = 4 per group) and lung (n = 2 per group). Scale bar, 2 mm.

All data are presented as means  $\pm$  SEM. Analysis was performed using two-way ANOVA followed by Bonferroni's post hoc test (\*p < 0.05; \*\*p < 0.01; \*\*\*p < 0.001).

function and in the production of complement, chemokines, and cytokines.

**Regional Endothelial Response but Preserved BBB Integrity in the Brain of TNFtg Mice**

Subsequently, we sought for the anatomical routes conveying the regional inflammatory response into the brain of TNFtg mice. We

*Nfkbia*, *Itgax* (Cd11c), and *Axl* (Figure 4G). A comparison of TNFtg microglia and inflammatory macrophages (cluster 2) showed that many of these gene expression changes are in the same trajectory but more pronounced in inflammatory macrophages. Genes belonging to complement factors (*C3*, *C1qa*, and *C1qc*), chemokines (*Cxcl13* and *Cxcl16*) and cytokines (*Ccl2* and *Ccl12*) were enriched in the inflammatory macrophage cluster (Figure 4H; Table S5). Tetraspanins are a large superfamily of cell-surface-associated membrane proteins, and they participate in a variety of cellular processes such as cell activation and differentiation. The tetraspanins Cd9 and Cd63 were enriched in inflammatory macrophage cluster. Cd63 is associated with membranes of intracellular vesicles (e.g., lysosomes). Lamp2, which plays an important role in chaperone-mediated autophagy and is thereby involved in lysosomal degradation of proteins in response to stress, was upregulated in cluster 2. *Tyrobp*, a gene playing a role in signal transduction, brain myelination, and inflammation, was downregulated. However, its putative receptor, Trem2, was not altered (Figure 4H). Gene set enrichment analysis of cluster-2-specific genes revealed significant involvement in genes associated with lysosomes, ATP metabolic process, and response to interferon gamma (Figure S6). Taken together, systemic chronic inflammation altered the myeloid cell composition in the cortex and resulted in the induction of a distinct population of inflammatory macrophages that are characterized by the downregulation of homeostatic microglia markers and the induction of genes involved in lysosomal

therefore quantified CD169<sup>+</sup> leptomeningeal macrophages adjacent to the cortex and cerebellum of WT and TNFtg mice, respectively. While the number of leptomeningeal macrophages was increased in vicinity to the cortex of TNFtg mice, there were no differences in the meninges surrounding the cerebellum (Figure S7A). This suggests that leptomeninges are involved in the regional immune response.

However, as the thalamus and striatum are devoid of meninges, we hypothesized that regional immune-to-brain communication might be exerted via regional alterations of the BBB. As such, we looked for regional modulation caused by the endothelial cells of the BBB in the cortex, striatum, thalamus, hippocampus, and cerebellum of TNFtg mice. We tested regional tight junction integrity to detect disruption of the BBB. However, there were no differences in *Cldn5* and *Tjp1* mRNA levels between WT and TNFtg mice in any of the brain regions analyzed (Figure 5A). Regional confocal colocalization analysis of Cldn5<sup>+</sup> tight junctions on CD31<sup>+</sup> blood vessels performed according to a previously published approach (Watkins et al., 2014) did not show any difference of vascular tight junction coverage (Figure 5B).

To assess the permeability, we injected Evans blue intravenously into WT and TNFtg mice and determined dye content in dissected brain regions 24 h later (Figure 5C). We did not observe any difference in Evans blue signal in the cortex, striatum, thalamus, hippocampus, or cerebellum between WT and TNFtg mice, further supporting the absence of regional BBB tight junction leakage (Figure 5C). In contrast, Evans blue permeability

(E) Donut plots showing the proportion of each group of cells to the experimental groups.

(F) t-SNE plots and violin plots depicting selected genes for microglia homeostasis markers.

(G) t-SNE plots and violin plots for selected genes for upregulated genes in inflammatory macrophages compared to WT microglia genes.

(H) Selected examples of violin plots. IM, inflammatory macrophages; MO, monocytes; GR, granulocytes.

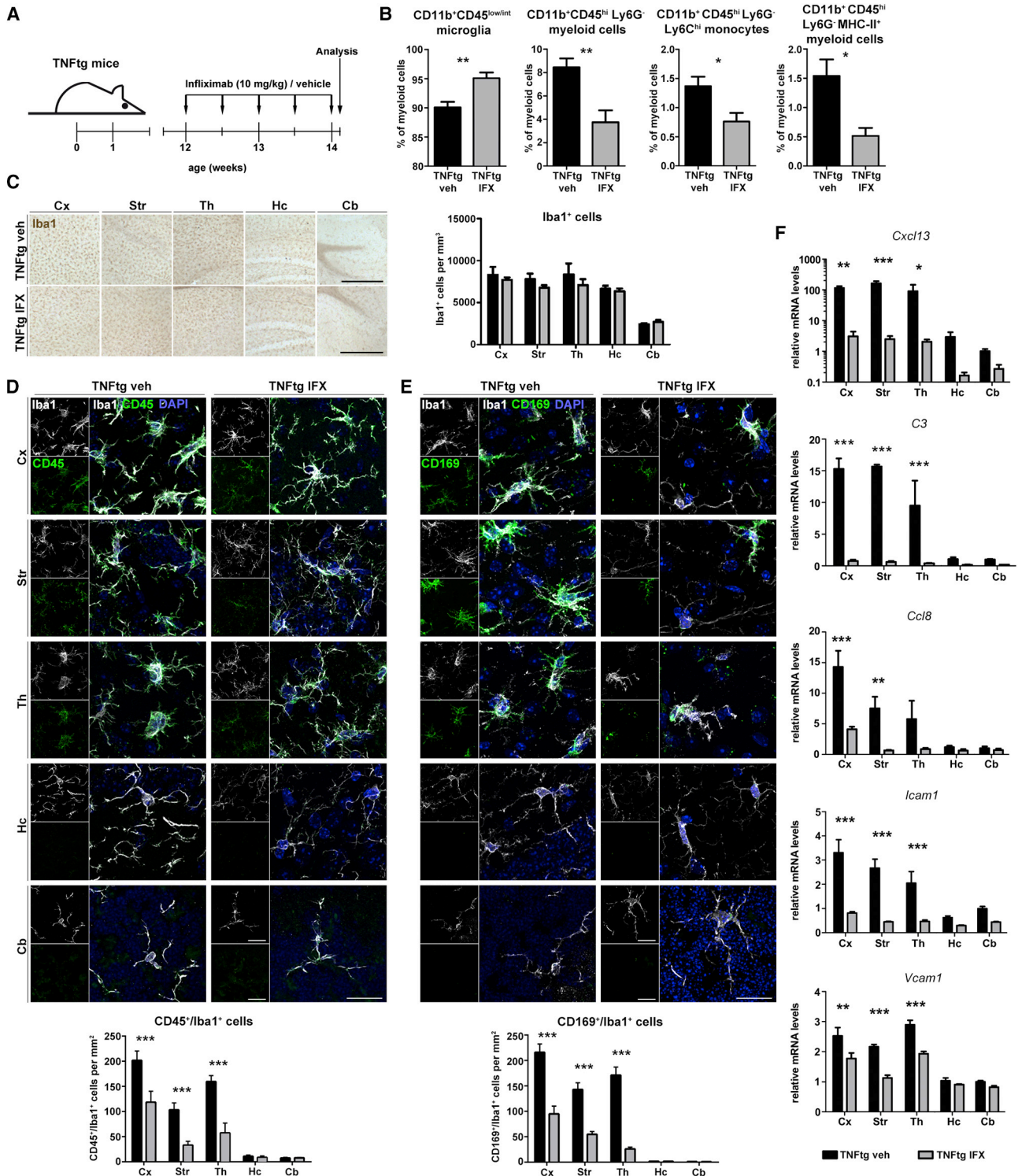


**Figure 6. Reversal of Regional CNS Myeloid Cell Activation and Transcriptional Response by Peripheral Human TNF- $\alpha$  Inhibition**

(A) Infliximab (IFX) treatment paradigm.

(B) Flow cytometry analysis of myeloid cells in the whole brain following the gating strategy displayed in Figure S1 (n = 5 per group).

(C) Densities of Iba1<sup>+</sup> cells in the cortex (Cx), striatum (Str), thalamus (Th), hippocampus (Hc), and cerebellum (Cb) of TNFtg mice treated with IFX or vehicle (n = 4 per group). Scale bars, 500  $\mu$ m.

(legend continued on next page)

was significantly increased in lung tissue of injected WT mice (Figures 5C and S7D). In line with this, regional extravascular leakage of albumin and fibrinogen into the CNS parenchyma was not detected by confocal microscopy in the cortex and cerebellum (Figures S7B and S7C). These findings suggest that there are no regional differences in BBB integrity induced by chronic innate peripheral inflammation in TNFtg mice.

We next wondered whether regional nondisruptive alterations of the BBB are detected in TNFtg mice (Varatharaj and Galea, 2017). We therefore investigated the expression of the endothelial activation markers and leukocyte adhesion molecules *Icam1* and *Vcam1*. Consistent with our bulk RNA-seq data (Table S2), qPCR analysis showed an increase of *Icam1* and *Vcam1* mRNA levels preferentially in the cortex, striatum, and thalamus of TNFtg mice (Figure S4C). Levels of *Icam1* mRNA were also increased in the hippocampus and cerebellum of TNFtg mice, though to a lower extent. These data indicate that despite intact global BBB integrity, we cannot rule out regional activation of BBB endothelial cells, which may contribute to the regional inflammatory response in the brain of TNFtg mice (e.g., by facilitating regional infiltration of blood-derived myeloid cells or secreting proinflammatory mediators) (Blank et al., 2016; Yousef et al., 2019).

### TNF- $\alpha$ Inhibition Reverses Regional CNS Response to Innate Peripheral Inflammation

Next, we asked whether regional CNS myeloid and endothelial cell activation in the brains of TNFtg mice is reversed by blocking human TNF- $\alpha$ . We therefore injected IFX, a monoclonal antibody against human TNF- $\alpha$ , at the age of 12–14 weeks (Figure 6A), when robust inflammation and monocyte-derived cell infiltration were already present in the cortex of TNFtg mice (Paouri et al., 2017; Süß, 2017). Intriguingly, flow cytometry of whole-brain homogenates showed that IFX treatment led to an increase in the ratio of CD11b<sup>+</sup>CD45<sup>low/int</sup> microglia compared to untreated TNFtg mice (Figure 6B), indicating the recovery of a microglial population to a resting state. Accordingly, IFX strongly reduced the proportion of CD11b<sup>+</sup>CD45<sup>hi</sup>Ly6G<sup>-</sup> myeloid cells in the brain of TNFtg mice (Figure 6B). This reduction of the CD11b<sup>+</sup>CD45<sup>hi</sup> myeloid cell population included a decrease in the proportions of Ly6C<sup>hi</sup> monocyte-derived cells (Figure 6B) as well as MHC-II<sup>+</sup> myeloid cells (Figure 6B).

Moreover, we investigated the regional effects of IFX treatment on myeloid cell response to obtain a spatial resolution of IFX effects in the brain of TNFtg mice. While there were no significant differences in the density of Iba1<sup>+</sup> cells between vehicle- and IFX-treated TNFtg mice in any brain regions analyzed (Figure 6C), the co-expression of the activation markers CD45 (Figure 6D) and CD169 (Figure 6E) was markedly reduced in the cortex, striatum, and thalamus by IFX treatment.

Subsequently, by regional qPCR analysis, we observed that the profound induction of *Cxcl13* and *C3* in the cortex, striatum,

and thalamus of TNFtg mice was almost completely reversed by IFX treatment in these three brain regions (Figure 6F). In contrast, there were only limited changes in the comparatively low mRNA levels of *Cxcl13* and *C3* in the cerebellum and hippocampus of TNFtg mice treated with IFX (Figure 6F). Additionally, the upregulation of *Icam1* and *Vcam1* mRNA was significantly reduced in the cortex, striatum, and thalamus of IFX-treated TNFtg mice (Figure 6F).

These data show that inhibition of long-lasting innate inflammation in the periphery is sufficient to restore the regional myeloid cell response and transcriptional inflammatory signature in the brain of TNFtg mice. The region-specific treatment response is similar for the cortex, striatum, and thalamus.

### Region-Specific Disruption of Myeloid Cell Homeostasis in RA Patients

Having detected a regional inflammatory response in a mouse model of RA, we wondered if a regionally distinct immune fingerprint is present in the brain of RA patients. To this end, we investigated cortical and cerebellar postmortem brain tissue of RA patients and age-matched controls (Figure 7A; Table S6) by immunohistochemistry for IBA1, which we found was increased in the cortex of TNFtg mice, and the microglial signature marker P2RY12 (Figure 7B), which was transcriptionally downregulated in the cortex of TNFtg mice (Figure 3H; Table S2). The numbers of IBA1<sup>+</sup> cells and P2RY12<sup>+</sup> homeostatic microglia were not different between controls and RA tissue in the cerebellum and cortex (Figure 7C). However, the ratio of P2RY12<sup>+</sup>/IBA1<sup>+</sup> cells was significantly decreased in the cortex of individuals with RA compared to controls (Figure 7C). Despite potentially confounding comorbidities of individual patients, this regional decrease in the proportion of homeostatic microglia may suggest a brain-region-specific response in RA patients similar to our observation in a mouse model for RA.

## DISCUSSION

The response of anatomical brain regions and specifically that of microglia to chronic peripheral inflammatory stimuli is largely unexplored territory. Here, we provide a thorough spatial resolution of immune-to-brain communication in the context of chronic inflammation. Specifically, we show modulation of the microglia gene expression signature to progressive peripheral overexpression of human TNF- $\alpha$ , which was reversible after peripherally antagonizing TNF- $\alpha$ . We provide evidence derived from post-mortem brain tissue of patients with RA that the brain myeloid cell compartment is affected in a brain-region-specific manner.

To study the effect of chronic peripheral inflammation, we leveraged the TNFtg mouse model, which overexpresses human TNF- $\alpha$  in the periphery, characterized by inflammatory joint pathology and elevated levels of cytokines in the blood (Keffer et al., 1991; Schett et al., 2003). Human TNF- $\alpha$  in the CNS of

(D and E) Co-expression of CD45 (D) and CD169 (E) in parenchymal myeloid cells in the cortex, striatum, and thalamus of TNFtg mice after treatment with IFX or vehicle (n = 4 per group). Scale bars, 10  $\mu$ m.

(F) Regional expression of *Cxcl13*, *C3*, *Ccl8*, *Icam1* and *Vcam1* mRNA levels in the brain regions of TNFtg mice after IFX or vehicle treatment.

All data are presented as means  $\pm$  SEM. Statistical analysis was performed using unpaired Student's t test (B) or two-way ANOVA followed by Bonferroni's post hoc test (C–F) (\*p < 0.05; \*\*p < 0.01; \*\*\*p < 0.001).

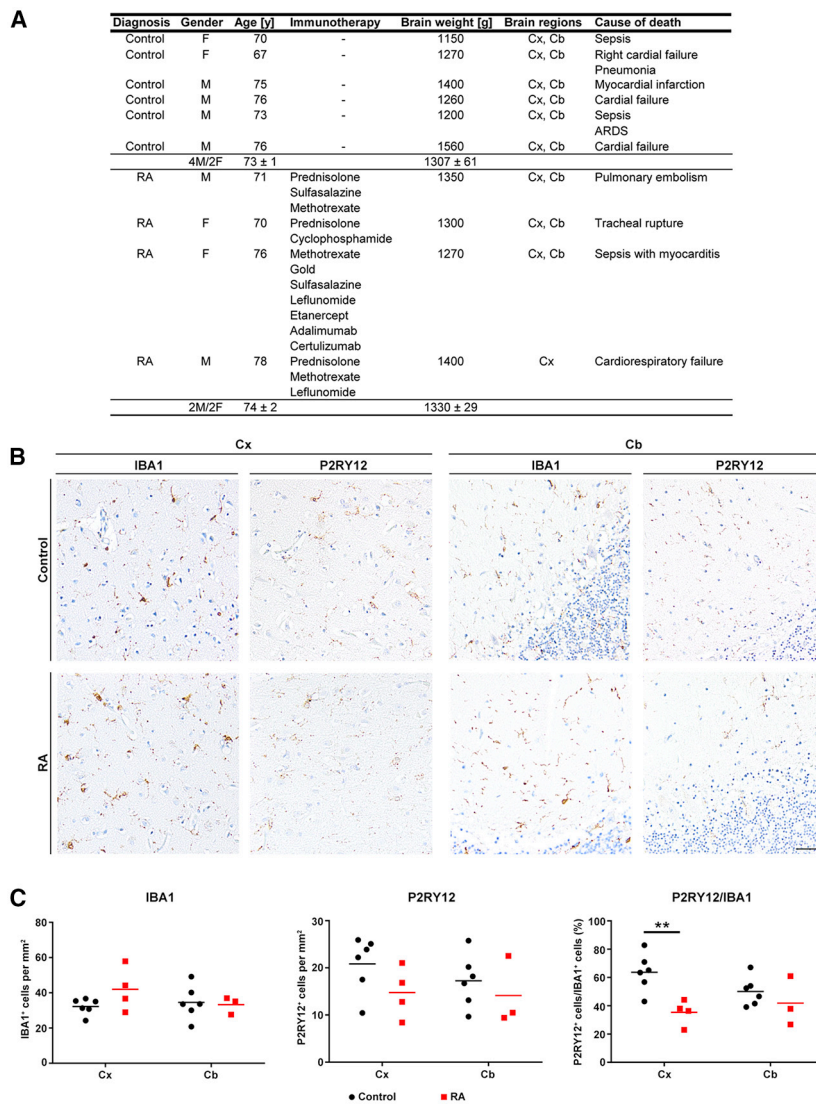


**Figure 7. Regional Microglial Response in the Cortex of Rheumatoid Arthritis Patients Revealed by Immunohistochemistry of Human Postmortem Brain Tissue**

(A) Overview showing main characteristics of rheumatoid arthritis (RA) patients (n = 4) and controls (n = 6). (B) Representative images depicting immunohistochemistry for IBA1 and P2RY12 in the cortex (Cx) and cerebellum (Cb) of RA patients and controls. Scale bar, 50  $\mu$ m. (C) Scatterplots indicating densities of IBA1<sup>+</sup> total microglia (left), P2RY12<sup>+</sup> homeostatic microglia (middle), and the percentage of P2RY12<sup>+</sup> homeostatic microglia normalized to IBA1<sup>+</sup> total microglia (right) in the cortex and cerebellum of RA patients and controls. Data are indicated as means  $\pm$  SEM and were analyzed using two-way ANOVA followed by Bonferroni's post hoc test (\*\*p < 0.01). M, male; F, female; ARDS, acute respiratory distress syndrome.

myeloid cells in the context of chronic peripheral inflammation is unclear.

We observed heterogeneity in the response of microglia to persistent peripheral inflammation, with the strongest response in the cortex, striatum, and thalamus, while almost absent in the hippocampus and cerebellum. Several reasons may account for this striking finding. First, the environment of the respective site could shape the microglia response to chronic peripheral inflammation. The enhancer landscapes of both murine and human microglia are shaped by local brain environmental cues (Gosselin et al., 2014, 2017). Cytokines like TNF- $\alpha$  and type I interferons are able to further modulate gene regulatory elements in a cooperative fashion to induce either long-term pro-inflammatory gene expression or immune tolerance (Park et al., 2017). Recently, innate immune

TNFTg mice was absent or only minimally detectable on protein (Süß et al., 2015) or mRNA levels (Figure S4). Moreover, human TNF- $\alpha$  protein does not cross the murine BBB (Banks et al., 1998). Thus, TNFTg mice serve as a model of peripheral progressive inflammation.

In response to the persistent inflammatory challenge, we detected a distinct microglia cluster that showed an increased inflammatory phenotype. Specifically, this population was characterized by the downregulation of homeostatic microglia markers such as *Fcrls* and *Cx3cr1*. Genes for complement (*C3* and *C1qc*) and chemokines (*Cxcl13* and *Cxcl16*) were upregulated. We also observed genes reminiscent of a previously identified microglia cluster that is associated with aging and neurodegenerative diseases such as AD (Keren-Shaul et al., 2017; Krasemann et al., 2017). These genes include *Tyrbp*, *Ctsb*, *ApoE*, *Fth1*, *Axl*, *Cd9*, and *Itgax*. The corresponding cell population may show increased phago-lysosomal activity, oxidative phosphorylation, and antigen-presentation functions. However, the role of these

memory and tolerance of microglia were identified as pivotal shapers of neurological disease (Wendeln et al., 2018). It is tempting to speculate that cytokine-induced chromatin refinement and precedent distinctive regional gene regulatory elements might be integrated to induce or prevent regional CNS inflammation in TNFTg mice. The regional composition of neuronal subtypes and neurotransmitter profiles is able to modulate microglial responses (Kettenmann et al., 2011; Lee, 2013). Of note, microenvironmental influences of microglia seem to be highly conserved, as different phenotypes of microglia from distinct basal ganglia substructures were reestablished in repopulating cells after microglial depletion induced by diphtheria toxin and colony-stimulating factor 1 receptor (Csf1r) inhibition (De Biase et al., 2017). Apart from resident immune cells, the local environment of different organs affected the inflammatory phenotype of infiltrating monocyte-derived cells (Spath et al., 2017). Interestingly, the regional immune fingerprint in TNFTg mice resembles the transcriptional heterogeneity of microglia

under steady-state conditions detected by microarray analysis, indicating high similarities between cortical and striatal microglia in comparison to the hippocampus and cerebellum (Grabert et al., 2016). By implication, our data indicate a baseline immunophenotype of the thalamus similar to the cortex and striatum. Mass cytometry of human microglia showed an activated signature in the thalamus, while cerebellar microglia had a distinct phenotype compared to other brain regions (Böttcher et al., 2019). Cerebellar microglia identity depends on CSF-1 in contrast to forebrain microglia, which depend on interleukin-34 (IL-34) (Kana et al., 2019). A unique role of cerebellar immune responses is further supported by a distinct cerebellar transcription pattern of microglia-specific genes altered during aging compared to nine other human brain regions (Soreq et al., 2017).

Asking for the anatomical route conveying regional immune responses in TNFtg mice, we detected an increase in the density of leptomeningeal macrophages on the surface of the cortex, but not the cerebellum. Leptomeninges might therefore contribute to the regional inflammatory propagation observed but cannot serve as the only route, as they are not in close proximity to the thalamus and striatum. Likewise, the choroid plexus is unlikely to mediate regional inflammation in TNFtg mice, since it is located near the hippocampus but more distant from the cortex. Instead, our findings imply regional propagation of peripheral inflammation by BBB endothelial cells. Several recent findings underline the role of endothelial Icam1 and Vcam1 in transducing systemic immune signals into the CNS (Beazley-Long et al., 2018; Langert et al., 2013; Yousef et al., 2019). Future research will be required to confirm the role of BBB endothelial cells in the context of RA and understand their regional modulation and whether BBB endothelial cells show a pattern similar to a recently described common gene expression signature in BBB dysfunction (Munji et al., 2019). Besides interfaces between the periphery and the CNS, sophisticated multimodal MRI analyses provided evidence for profound alterations in interregional connectivity within the brains of RA patients, which could also be linked to regional inflammatory signatures (Schrepf et al., 2018).

We show that the regional inflammatory response in the brain of TNFtg mice is efficiently reversed by IFX. IFX does not cross the BBB (Bohren et al., 2013; Paouri et al., 2017) and rescues cortical inflammation observed in TNFtg mice (Bohren et al., 2013; Paouri et al., 2017; Süß, 2017). In mice and human, IFX treatment rapidly reduces pain induced by arthritis (Hess et al., 2011). Based on fMRI studies, TNFtg mice and RA patients show increased blood flow in the thalamus and cortical areas, which is restored after short IFX treatment (Hess et al., 2011). Although future studies will be required to correlate these fMRI findings with regional immunological heterogeneity in the brain and reveal potential rapid effects of IFX on an immunological level, our data indicate that the reversal of regional CNS inflammation might provide a pivotal target to rapidly modulate responses to chronic pain in other diseases with chronic peripheral inflammation.

Insights into the impact of chronic peripheral inflammation on the human brain are very limited. We provide analyses of post-mortem brain tissue of RA patients, strongly indicating that regional CNS myeloid cell response occurs in patients with chronic peripheral inflammatory diseases. In summary, we pro-

vide strong evidence that the steady-state immunological heterogeneity of different brain regions, which is yet to be precisely deciphered, is driving distinct responses to chronic peripheral inflammation in mice and humans. Taking into account even sub-regional differences in microglial phenotypes, future studies on the bidirectional crosstalk between the CNS and the peripheral immune system require thorough neuroanatomical dissection. Our study indicates that chronic peripheral inflammation induces distinct changes in the myeloid cell compartment in the CNS of individuals; however, the contribution of these changes to the development of neuropsychiatric and neurodegenerative disorders is still an open question.

## STAR★METHODS

Detailed methods are provided in the online version of this paper and include the following:

- KEY RESOURCES TABLE
- LEAD CONTACT AND MATERIALS AVAILABILITY
- EXPERIMENTAL MODEL AND SUBJECT DETAILS
  - Animals
  - Human Postmortem Brain Tissue
- METHOD DETAILS
  - Murine Tissue Processing and Immunostainings
  - Histological Quantification
  - Evans Blue Assay
  - Isolation and Immunophenotyping of CNS Myeloid Cells
  - RNA Isolation and qPCR
  - Region-Specific Bulk RNA Sequencing
  - Differential Gene Expression and Variability Analysis
  - Single Cell RNA Sequencing
  - Immunohistochemistry of Human Postmortem Tissue
- QUANTIFICATION AND STATISTICAL ANALYSIS
- DATA AND CODE AVAILABILITY

## SUPPLEMENTAL INFORMATION

Supplemental Information can be found online at <https://doi.org/10.1016/j.celrep.2020.02.109>.

## ACKNOWLEDGMENTS

We thank L. Van Ael for her assistance with preparing the graphical abstract. We also thank George Kollias (Fleming Institute, Vari, Greece) for providing TNFtg mice. The present work was funded by the NIH grant R01 AG061060-01, Deutsche Forschungsgemeinschaft (DFG, Germany; INST 410/45-1 FUGG) and the Interdisciplinary Center for Clinical Research (IZKF, Erlangen, Germany, project E24). J.W., P.S., and A.H. are members of research training group GRK2162 funded by the DFG (270949263/GRK2162). P.S. is supported by the University Hospital Erlangen (Germany, ELAN project P059, IZKF clinician scientist program). J.C.M.S. is supported by the DFG (research grant SCHL 21021-1). The work of G.S. and G.K. is supported by the DFG (CRC1181), an ERC starting grant to G.K., and the Innovative Medicine Initiative project RT-Cure.

## AUTHOR CONTRIBUTIONS

Conceptualization, P.S. and J.C.M.S.; Investigation, P.S., A.H., T.R., and J.C.M.S.; Resources, W.B., G.S., G.K., M.P., C.K.G., and J.W.; Formal

Analysis, P.S., A.H., O.S., Z.O., and J.C.M.S.; Writing – Original Draft, P.S.; Writing – Review & Editing, A.H., J.W., and J.C.M.S.; Supervision, M.P., C.K.G., J.W., and J.C.M.S.

## DECLARATION OF INTERESTS

The authors declare no competing interests.

Received: September 22, 2018

Revised: January 15, 2020

Accepted: February 27, 2020

Published: March 24, 2020

## REFERENCES

- Aran, D., Looney, A.P., Liu, L., Wu, E., Fong, V., Hsu, A., Chak, S., Naikawadi, R.P., Wolters, P.J., Abate, A.R., et al. (2019). Reference-based analysis of lung single-cell sequencing reveals a transitional profibrotic macrophage. *Nat. Immunol.* **20**, 163–172.
- Ayata, P., Badimon, A., Strasburger, H.J., Duff, M.K., Montgomery, S.E., Loh, Y.E., Ebert, A., Pimenova, A.A., Ramirez, B.R., Chan, A.T., et al. (2018). Epigenetic regulation of brain region-specific microglia clearance activity. *Nat. Neurosci.* **21**, 1049–1060.
- Balusu, S., Van Wonterghem, E., De Rycke, R., Raemdonck, K., Stremersch, S., Gevaert, K., Brkic, M., Demeestere, D., Vanhooren, V., Hendrix, A., et al. (2016). Identification of a novel mechanism of blood-brain communication during peripheral inflammation via choroid plexus-derived extracellular vesicles. *EMBO Mol. Med.* **8**, 1162–1183.
- Banks, W.A., Kastin, A.J., and Ehrensing, C.A. (1998). Diurnal uptake of circulating interleukin-1alpha by brain, spinal cord, testis and muscle. *Neuroimmunomodulation* **5**, 36–41.
- Beazley-Long, N., Moss, C.E., Ashby, W.R., Bestall, S.M., Almahasneh, F., Durrant, A.M., Benest, A.V., Blackley, Z., Ballmer-Hofer, K., Hirashima, M., et al. (2018). VEGFR2 promotes central endothelial activation and the spread of pain in inflammatory arthritis. *Brain Behav. Immun.* **74**, 49–67.
- Bennett, M.L., Bennett, F.C., Liddel, S.A., Ajami, B., Zamanian, J.L., Fernhoff, N.B., Mulinyaw, S.B., Bohlen, C.J., Adil, A., Tucker, A., et al. (2016). New tools for studying microglia in the mouse and human CNS. *Proc. Natl. Acad. Sci. U S A* **113**, E1738–E1746.
- Blank, T., Detje, C.N., Spieß, A., Hagemeyer, N., Brendecke, S.M., Wolfart, J., Staszewski, O., Zöller, T., Papageorgiou, I., Schneider, J., et al. (2016). Brain endothelial- and epithelial-specific interferon receptor chain 1 drives virus-induced sickness behavior and cognitive impairment. *Immunity* **44**, 901–912.
- Bohren, Y., Tessier, L.H., Megat, S., Petitjean, H., Hugel, S., Daniel, D., Kremer, M., Fournel, S., Hein, L., Schlichter, R., et al. (2013). Antidepressants suppress neuropathic pain by a peripheral  $\beta$ 2-adrenoceptor mediated anti-TNF $\alpha$  mechanism. *Neurobiol. Dis.* **60**, 39–50.
- Böttcher, C., Schlickeiser, S., Sneeboer, M.A.M., Kunkel, D., Knop, A., Paza, E., Fidzinski, P., Kraus, L., Snijders, G.J.L., Kahn, R.S., et al.; NBB-Psy (2019). Human microglia regional heterogeneity and phenotypes determined by multiplexed single-cell mass cytometry. *Nat. Neurosci.* **22**, 78–90.
- Capuron, L., and Miller, A.H. (2011). Immune system to brain signaling: neuropsychopharmacological implications. *Pharmacol. Ther.* **130**, 226–238.
- Chou, R.C., Kane, M., Ghimire, S., Gautam, S., and Gui, J. (2016). Treatment for rheumatoid arthritis and risk of Alzheimer's disease: a nested case-control analysis. *CNS Drugs* **30**, 1111–1120.
- Czirr, E., and Wyss-Coray, T. (2012). The immunology of neurodegeneration. *J. Clin. Invest.* **122**, 1156–1163.
- D'Mello, C., and Swain, M.G. (2017). Immune-to-brain communication pathways in inflammation-associated sickness and depression. *Curr. Top. Behav. Neurosci.* **37**, 73–94.
- Dantzer, R., Capuron, L., Irwin, M.R., Miller, A.H., Ollat, H., Perry, V.H., Rousey, S., and Yirmiya, R. (2008a). Identification and treatment of symptoms associated with inflammation in medically ill patients. *Psychoneuroendocrinology* **33**, 18–29.
- Dantzer, R., O'Connor, J.C., Freund, G.G., Johnson, R.W., and Kelley, K.W. (2008b). From inflammation to sickness and depression: when the immune system subjugates the brain. *Nat. Rev. Neurosci.* **9**, 46–56.
- De Biase, L.M., Schuebel, K.E., Fufeld, Z.H., Jair, K., Hawes, I.A., Cimbri, R., Zhang, H.Y., Liu, Q.R., Shen, H., Xi, Z.X., et al. (2017). Local cues establish and maintain region-specific phenotypes of basal ganglia microglia. *Neuron* **95**, 341–356.e6.
- Dobin, A., Davis, C.A., Schlesinger, F., Drenkow, J., Zaleski, C., Jha, S., Batut, P., Chaisson, M., and Gingeras, T.R. (2013). STAR: ultrafast universal RNA-seq aligner. *Bioinformatics* **29**, 15–21.
- Fourgeaud, L., Través, P.G., Tufail, Y., Leal-Bailey, H., Lew, E.D., Burrola, P.G., Callaway, P., Zagórska, A., Rothlin, C.V., Nimmerjahn, A., and Lemke, G. (2016). TAM receptors regulate multiple features of microglial physiology. *Nature* **532**, 240–244.
- Furube, E., Kawai, S., Inagaki, H., Takagi, S., and Miyata, S. (2018). Brain region-dependent heterogeneity and dose-dependent difference in transient microglia population increase during lipopolysaccharide-induced inflammation. *Sci. Rep.* **8**, 2203.
- Gao, L., Brenner, D., Llorens-Bobadilla, E., Saiz-Castro, G., Frank, T., Wieghofer, P., Hill, O., Thiemann, M., Karray, S., Prinz, M., et al. (2015). Infiltration of circulating myeloid cells through CD95L contributes to neurodegeneration in mice. *J. Exp. Med.* **212**, 469–480.
- Goldmann, T., Wieghofer, P., Jordão, M.J., Prutek, F., Hagemeyer, N., Frenzel, K., Amann, L., Staszewski, O., Kierdorf, K., Krueger, M., et al. (2016). Origin, fate and dynamics of macrophages at central nervous system interfaces. *Nat. Immunol.* **17**, 797–805.
- Gosselin, D., Link, V.M., Romanoski, C.E., Fonseca, G.J., Eichenfield, D.Z., Spann, N.J., Stender, J.D., Chun, H.B., Garner, H., Geissmann, F., and Glass, C.K. (2014). Environment drives selection and function of enhancers controlling tissue-specific macrophage identities. *Cell* **159**, 1327–1340.
- Gosselin, D., Skola, D., Coufal, N.G., Holtman, I.R., Schlachetzki, J.C.M., Sajti, E., Jaeger, B.N., O'Connor, C., Fitzpatrick, C., Pasillas, M.P., et al. (2017). An environment-dependent transcriptional network specifies human microglia identity. *Science* **356**, 356.
- Grabert, K., Michoel, T., Karavolos, M.H., Clohisey, S., Baillie, J.K., Stevens, M.P., Freeman, T.C., Summers, K.M., and McColl, B.W. (2016). Microglial brain region-dependent diversity and selective regional sensitivities to aging. *Nat. Neurosci.* **19**, 504–516.
- Hammond, T.R., Dufort, C., Dissing-Olesen, L., Giera, S., Young, A., Wysoker, A., Walker, A.J., Gergits, F., Segel, M., Nemes, J., et al. (2019). Single-cell RNA sequencing of microglia throughout the mouse lifespan and in the injured brain reveals complex cell-state changes. *Immunity* **50**, 253–271.e256.
- Heinz, S., Benner, C., Spann, N., Bertolino, E., Lin, Y.C., Laslo, P., Cheng, J.X., Murre, C., Singh, H., and Glass, C.K. (2010). Simple combinations of lineage-determining transcription factors prime cis-regulatory elements required for macrophage and B cell identities. *Mol. Cell* **38**, 576–589.
- Hess, A., Axmann, R., Rech, J., Finzel, S., Heindl, C., Kreitz, S., Sergeeva, M., Saake, M., Garcia, M., Kollias, G., et al. (2011). Blockade of TNF- $\alpha$  rapidly inhibits pain responses in the central nervous system. *Proc. Natl. Acad. Sci. USA* **108**, 3731–3736.
- Hickman, S.E., Kingery, N.D., Ohsumi, T.K., Borowsky, M.L., Wang, L.C., Means, T.K., and El Khoury, J. (2013). The microglial sensome revealed by direct RNA sequencing. *Nat. Neurosci.* **16**, 1896–1905.
- Hoogland, I.C., Houbolt, C., van Westerloo, D.J., van Gool, W.A., and van de Beek, D. (2015). Systemic inflammation and microglial activation: systematic review of animal experiments. *J. Neuroinflammation* **12**, 114.
- Joyce, P.I., Fratta, P., Landman, A.S., McGoldrick, P., Wackerhage, H., Groves, M., Busam, B.S., Galino, J., Corrochano, S., Beskina, O.A., et al. (2016). Deficiency of the zinc finger protein ZFP106 causes motor and sensory neurodegeneration. *Hum. Mol. Genet.* **25**, 291–307.

- Kana, V., Desland, F.A., Casanova-Acebes, M., Ayata, P., Badimon, A., Nabel, E., Yamamuro, K., Sneuboer, M., Tan, I.L., Flanigan, M.E., et al. (2019). CSF-1 controls cerebellar microglia and is required for motor function and social interaction. *J. Exp. Med.* *216*, 2265–2281.
- Keffer, J., Probert, L., Cazlaris, H., Georgopoulos, S., Kaslaris, E., Kioussis, D., and Kollias, G. (1991). Transgenic mice expressing human tumour necrosis factor: a predictive genetic model of arthritis. *EMBO J.* *10*, 4025–4031.
- Keren-Shaul, H., Spinrad, A., Weiner, A., Matcovitch-Natan, O., Dvir-Szternfeld, R., Ulland, T.K., David, E., Baruch, K., Lara-Astaiso, D., Toth, B., et al. (2017). A unique microglia type associated with restricting development of Alzheimer's disease. *Cell* *169*, 1276–1290.e17.
- Kettenmann, H., Hanisch, U.K., Noda, M., and Verkhratsky, A. (2011). Physiology of microglia. *Physiol. Rev.* *91*, 461–553.
- Kierdorf, K., Masuda, T., Jordão, M.J.C., and Prinz, M. (2019). Macrophages at CNS interfaces: ontogeny and function in health and disease. *Nat. Rev. Neurosci.* *20*, 547–562.
- Kim, W.G., Mohny, R.P., Wilson, B., Jeohn, G.H., Liu, B., and Hong, J.S. (2000). Regional difference in susceptibility to lipopolysaccharide-induced neurotoxicity in the rat brain: role of microglia. *J. Neurosci.* *20*, 6309–6316.
- Kloss, C.U., Bohatschek, M., Kreutzberg, G.W., and Raivich, G. (2001). Effect of lipopolysaccharide on the morphology and integrin immunoreactivity of ramified microglia in the mouse brain and in cell culture. *Exp. Neurol.* *168*, 32–46.
- Krämer, A., Green, J., Pollard, J., Jr., and Tugendreich, S. (2014). Causal analysis approaches in Ingenuity Pathway Analysis. *Bioinformatics* *30*, 523–530.
- Krasemann, S., Madore, C., Cialic, R., Baufeld, C., Calcagno, N., El Fatimy, R., Beckers, L., O'Loughlin, E., Xu, Y., Fanek, Z., et al. (2017). The TREM2-APOE pathway drives the transcriptional phenotype of dysfunctional microglia in neurodegenerative diseases. *Immunity* *47*, 566–581.e9.
- Langert, K.A., Von Zee, C.L., and Stubbs, E.B., Jr. (2013). Tumour necrosis factor  $\alpha$  enhances CCL2 and ICAM-1 expression in peripheral nerve microvascular endoneurial endothelial cells. *ASN Neuro* *5*, e00104.
- Lee, M. (2013). Neurotransmitters and microglial-mediated neuroinflammation. *Curr. Protein Pept. Sci.* *14*, 21–32.
- Love, M.I., Huber, W., and Anders, S. (2014). Moderated estimation of fold change and dispersion for RNA-seq data with DESeq2. *Genome Biol.* *15*, 550.
- Masuda, T., Sankowski, R., Staszewski, O., Böttcher, C., Amann, L., Sagar, Scheiwe, C., Nessler, S., Kunz, P., van Loo, G., et al. (2019). Spatial and temporal heterogeneity of mouse and human microglia at single-cell resolution. *Nature* *566*, 388–392.
- McInnes, I.B., and Schett, G. (2011). The pathogenesis of rheumatoid arthritis. *N. Engl. J. Med.* *365*, 2205–2219.
- Munji, R.N., Soung, A.L., Weiner, G.A., Sohet, F., Semple, B.D., Trivedi, A., Gimlin, K., Kotoda, M., Korai, M., Aydin, S., et al. (2019). Profiling the mouse brain endothelial transcriptome in health and disease models reveals a core blood-brain barrier dysfunction module. *Nat. Neurosci.* *22*, 1892–1902.
- Nerurkar, L., Siebert, S., McInnes, I.B., and Cavanagh, J. (2019). Rheumatoid arthritis and depression: an inflammatory perspective. *Lancet Psychiatry* *6*, 164–173.
- Paouri, E., Tzara, O., Kartalou, G.I., Zenelak, S., and Georgopoulos, S. (2017). peripheral tumor necrosis factor- $\alpha$  (TNF- $\alpha$ ) modulates amyloid pathology by regulating blood-derived immune cells and glial response in the brain of AD/TNF transgenic mice. *J. Neurosci.* *37*, 5155–5171.
- Park, S.H., Kang, K., Giannopoulos, E., Qiao, Y., Kang, K., Kim, G., Park-Min, K.H., and Ivshchik, L.B. (2017). Type I interferons and the cytokine TNF cooperatively reprogram the macrophage epigenome to promote inflammatory activation. *Nat. Immunol.* *18*, 1104–1116.
- Perry, V.H., Crocker, P.R., and Gordon, S. (1992). The blood-brain barrier regulates the expression of a macrophage sialic acid-binding receptor on microglia. *J. Cell Sci.* *101*, 201–207.
- Ponomarev, E.D., Veremeyko, T., Barteneva, N., Krichevsky, A.M., and Weiner, H.L. (2011). MicroRNA-124 promotes microglia quiescence and suppresses EAE by deactivating macrophages via the C/EBP- $\alpha$ -PU.1 pathway. *Nat. Med.* *17*, 64–70.
- Prinz, M., Priller, J., Sisodia, S.S., and Ransohoff, R.M. (2011). Heterogeneity of CNS myeloid cells and their roles in neurodegeneration. *Nat. Neurosci.* *14*, 1227–1235.
- Sankowski, R., Mader, S., and Valdés-Ferrer, S.I. (2015). Systemic inflammation and the brain: novel roles of genetic, molecular, and environmental cues as drivers of neurodegeneration. *Front. Cell. Neurosci.* *9*, 28.
- Schett, G., Redlich, K., Hayer, S., Zwerina, J., Bolon, B., Dunstan, C., Görtz, B., Schulz, A., Bergmeister, H., Kollias, G., et al. (2003). Osteoprotegerin protects against generalized bone loss in tumor necrosis factor-transgenic mice. *Arthritis Rheum.* *48*, 2042–2051.
- Schlachetzki, J.C., Grimm, T., Schlachetzki, Z., Ben Abdallah, N.M., Etle, B., Vohringer, P., Ferger, B., Winner, B., Nuber, S., and Winkler, J. (2016). Dopaminergic lesioning impairs adult hippocampal neurogenesis by distinct modification of alpha-synuclein. *J. Neurosci. Res.* *94*, 62–73.
- Schrepf, A., Kaplan, C.M., Ichesco, E., Larkin, T., Harte, S.E., Harris, R.E., Murray, A.D., Waiter, G.D., Clauw, D.J., and Basu, N. (2018). A multi-modal MRI study of the central response to inflammation in rheumatoid arthritis. *Nat. Commun.* *9*, 2243.
- Shi, J., Johansson, J., Woodling, N.S., Wang, Q., Montine, T.J., and Andreasson, K. (2010). The prostaglandin E2 E-prostanoid 4 receptor exerts anti-inflammatory effects in brain innate immunity. *J. Immunol.* *184*, 7207–7218.
- Soreq, L., Rose, J., Soreq, E., Hardy, J., Trabzuni, D., Cookson, M.R., Smith, C., Ryten, M., Patani, R., and Ule, J. UK Brain Expression Consortium; North American Brain Expression Consortium (2017). Major shifts in glial regional identity are a transcriptional hallmark of human brain aging. *Cell Rep.* *18*, 557–570.
- Spath, S., Komuczki, J., Hermann, M., Pelczar, P., Mair, F., Schreiner, B., and Becher, B. (2017). Dysregulation of the cytokine GM-CSF induces spontaneous phagocyte invasion and immunopathology in the central nervous system. *Immunity* *46*, 245–260.
- Süb, P. (2017). Remote control: impacts of peripheral tumor necrosis factor- $\alpha$  on Alzheimer disease-related pathology. *J. Neurosci.* *37*, 8045–8047.
- Süb, P., Kalinichenko, L., Baum, W., Reichel, M., Kornhuber, J., Loskarn, S., Etle, B., Distler, J.H., Schett, G., Winkler, J., et al. (2015). Hippocampal structure and function are maintained despite severe innate peripheral inflammation. *Brain Behav. Immun.* *49*, 156–170.
- Tripathi, S., Pohl, M.O., Zhou, Y., Rodriguez-Frandsen, A., Wang, G., Stein, D.A., Moulton, H.M., DeJesus, P., Che, J., Mulder, L.C., et al. (2015). Meta- and orthogonal integration of influenza “OMICs” data defines a role for UBR4 in virus budding. *Cell Host Microbe* *18*, 723–735.
- Uguz, F., Akman, C., Kucuksarac, S., and Tufekci, O. (2009). Anti-tumor necrosis factor- $\alpha$  therapy is associated with less frequent mood and anxiety disorders in patients with rheumatoid arthritis. *Psychiatry Clin. Neurosci.* *63*, 50–55.
- Varatharaj, A., and Galea, I. (2017). The blood-brain barrier in systemic inflammation. *Brain Behav. Immun.* *60*, 1–12.
- Wallin, K., Solomon, A., Kåreholt, I., Tuomilehto, J., Soininen, H., and Kivipelto, M. (2012). Midlife rheumatoid arthritis increases the risk of cognitive impairment two decades later: a population-based study. *J. Alzheimers Dis.* *31*, 669–676.
- Watkins, S., Robel, S., Kimbrough, I.F., Robert, S.M., Ellis-Davies, G., and Sontheimer, H. (2014). Disruption of astrocyte-vascular coupling and the blood-brain barrier by invading glioma cells. *Nat. Commun.* *5*, 4196.
- Wendeln, A.C., Degenhardt, K., Kaurani, L., Gertig, M., Ulas, T., Jain, G., Wagner, J., Häslér, L.M., Wild, K., Skodras, A., et al. (2018). Innate immune memory in the brain shapes neurological disease hallmarks. *Nature* *556*, 332–338.
- Wu, Z., Zhang, J., and Nakanishi, H. (2005). Leptomeningeal cells activate microglia and astrocytes to induce IL-10 production by releasing pro-inflammatory cytokines during systemic inflammation. *J. Neuroimmunol.* *167*, 90–98.
- Yousef, H., Czupalla, C.J., Lee, D., Chen, M.B., Burke, A.N., Zera, K.A., Zandstra, J., Berber, E., Lehallier, B., Mathur, V., et al. (2019). Aged blood impairs hippocampal neural precursor activity and activates microglia via brain endothelial cell VCAM1. *Nat. Med.* *25*, 988–1000.

## STAR★METHODS

### KEY RESOURCES TABLE

REAGENT or RESOURCE	SOURCE	IDENTIFIER
<b>Antibodies</b>		
rat anti-mouse CD45	Bio-Rad	Cat# MCA1388, RRID:AB_321729 Clone: IBL-3/16
rat anti-CD169	Bio-Rad	Cat# MCA947, RRID:AB_322322 Clone: MOMA-1
rabbit anti-ionized calcium binding adaptor molecule 1 (Iba1)	Wako	Cat# 019-19741, RRID:AB_839504
mouse anti-NeuN	Merck-Millipore	Cat# MAB377, RRID:AB_2298772 Clone: A60
goat anti-glial fibrillary acidic protein (GFAP, C-19)	Santa Cruz Biotech	Cat# sc-6170, RRID:AB_641021
rabbit anti-Olig2	Merck-Millipore	Cat# AB9610, RRID:AB_570666
goat anti-collagen IV	Merck-Millipore	Cat# AB769, RRID:AB_92262
rabbit anti-albumin	Abcam	Cat# ab19196, RRID:AB_449857
rabbit anti-fibrinogen	Dako	Cat# A008002, RRID:AB_578481
rat anti-CD31	Santa Cruz Biotech	Cat# sc-18916, RRID:AB_627028 <b>Clone: MEC 13.3</b>
mouse anti-claudin 5 (Cldn5)	Thermo Fisher Scientific	Cat# 35-2500, RRID:AB_2533200 <b>Clone: 4C3C2</b>
<b>TruStain fcX (anti-mouse CD16/32) Antibody</b>	BioLegend	Cat# 101320 Lot: B234518 Clone: 93
anti-CD11b (M1/70)	BioLegend	Cat# 101215 Lot: B272160 Clone: M1/70
anti-CD45 (30-F11)	BioLegend	Cat# 103133 Lot: B263588 Clone: 30-F11
anti-MHC-II (M5/114.15.2)	BioLegend	Cat# 107608 Lot: B130064 Clone: M5/114.15.2
anti-Ly6C (HK1.4)	BioLegend	Cat# 128022 Lot: B248739 Clone: HK1.4
anti-Ly6G (1A8)	BioLegend	Cat# 127616 Lot: B196548 Clone: 1A8
rabbit anti-IBA-1	Abcam	Cat# ab178846, RRID:AB_2636859 Clone: EPR 16588
rabbit anti-P2RY12, 1:1,500	Sigma-Aldrich	Cat# HPA014518, RRID:AB_2669027
donkey anti-rat, Alexa 488	Thermo Fisher Scientific	Cat# A21208, RRID:AB_2535794
donkey anti-mouse, Alexa 568	Thermo Fisher Scientific	Cat# A10037, RRID:AB_2534013
donkey anti-goat, Alexa 568	Thermo Fisher Scientific	Cat# A11057, RRID:AB_2534104
donkey anti-rabbit, Alexa 647	Thermo Fisher Scientific	Cat# A32795, RRID:AB_2762835
donkey anti-rabbit, biotin	Dianova	Cat# 711-066-152

(Continued on next page)

<i>Continued</i>		
REAGENT or RESOURCE	SOURCE	IDENTIFIER
Biological Samples		
Human cortical and cerebellar brain samples of RA patients and controls	Institute of Neuropathology, University of Freiburg	N/A
Chemicals, Peptides, and Recombinant Proteins		
DAPI	Sigma-Aldrich	<b>Cat# D8417-1mg</b>
ProLong Gold antifade reagent	Thermo Fisher Scientific	Cat# P36930
Evans Blue	Sigma-Aldrich	Cat# E2129-10G Lot# MKBK0523V
eBioscience eFluor 780 Fixable Viability Dye	eBioscience	<b>Cat# 65-0865-14</b>
Infliximab	Janssen Biotech, Inc.	Lot# S017485
Oligo d(T)25 Magnetic Beads	NEB	Cat# S1419S
Nuclease Free Water	Ambion	Cat# AM9930
Random Primers	Life Technology	Cat# 48190011
SUPERase-In	Ambion	Cat# AM2696
Actinomycin D	Sigma	Cat# A1410
DTT	Thermo Fisher Scientific	Cat#P2325
dNTP	Life Technology	Cat# 18427088
Superscript III Reverse Transcriptase	Life Technology	Cat# 18080-044
5X SuperScriptIII first-strand buffer	Life Technology	Cat# 18080-044
dNTPs (10mM with dUTP)	Affymetrix (Core)	77330
dUTP(100mM)	Affymetrix (Core)	77206
RNase H	Enzymatics	Y9220L
DNA polymerase I (E. Coli) with 10X blue Buffer	Enzymatics	P7050L
10X T4 ligase buffer	Enzymatics	B6030L
T4 DNA pol	Enzymatics	P7080L
Kenow	Enzymatics	P7060L
T4 PNK	Enzymatics	Y9040L
dNTP (25mM)	Affymetrix (Core)	77119
dATP mix (100mM)	Life Technology	10216-018
Klenow 3'-5' exo	Enzymatics	P7010-LC-L
T4 DNA Ligase	Enzymatics	L6030-HC-L
2X Rapid Ligation Buffer	Enzymatics	B1010L
Uracil DNA Glycosylase	Enzymatics	G5010L
RNA Clean XP	Beckman Coulter	A63987
Sera-Mag Speedbeads	Thermo Scientific	6515-2105-050250
10% TBE gel, 12 well	Life Technology	EC62752Box
Track It 25 bp ladder	Life Technology	T10488022
SYBR Gold Nucleic Acid Stain	Life Technology	S11494
NEXTflex DNA barcodes	Bioo Scientific	Cat#NOVA-514104
KAPA SYBR FAST qPCR Master mix (2X)	Kapa Biosystems	Cat#07959427001
TRIzol Reagent	Thermo Fisher Scientific	Cat# 15596018
Critical Commercial Assays		
VECTASTAIN® Elite® ABC HRP Kit (Peroxidase, Standard)	Vectastain	Cat# PK-6100
DAB Peroxidase (HRP) Substrate Kit (with Nickel), 3,3'-diaminobenzidine	Vectastain	Cat# SK-4100
RNeasy Plus Mini Kit	QIAGEN	Cat# 74136
GoScript Reverse Transcription System	Promega	Cat# A5004

(Continued on next page)

<b>Continued</b>		
REAGENT or RESOURCE	SOURCE	IDENTIFIER
EnVision FLEX, High pH (Link)	Agilent	Cat# K8000
ChIP DNA Clean & Concentrator Kit	ZymoResearch	Cat# D5205
Qubit DNA HS 100 Assay Kit (buffer)	Life Technology	Cat# Q32851
Deposited Data		
Raw and analyzed data	EMBL-EBI Expression Atlas	E-MTAB-7279
	GEO	GSE145708
RNaseq of brain regions from WT and TNFtg mice	EMBL-EBI Expression Atlas	E-MTAB-7279
scRNaseq of CD45+ cells from cortex of WT and TNFtg mice	GEO	GSE145708
Experimental Models: Organisms/Strains		
Mouse strain: Tg197 (hTNFtg)	George Kollias (Fleming Institute, Vari, Greece) <a href="#">Keffer et al., 1991; Süß et al., 2015</a>	Cat# 3053718, RRID:MGI:3053718
Oligonucleotides		
See <a href="#">Table S1</a>	This paper	N/A
Software and Algorithms		
StereoInvestigator software	MicroBrightField	N/A
ZEN Blue software	Zeiss	N/A
ZEN Black software	Zeiss	N/A
CytoFLEX	Beckman Coulter	N/A
FlowJo software (version 10)	TreeStar Inc.	N/A
Fiji	OlympusViewer Plugin	<a href="https://imagej.net/OlympusImageJPlugin">https://imagej.net/OlympusImageJPlugin</a>
Metascape	<a href="#">Tripathi et al., 2015</a>	<a href="http://metascape.org">http://metascape.org</a>
R package: Pheatmap	N/A	<a href="https://www.rdocumentation.org/packages/pheatmap/versions/1.0.10/topics/pheatmap">https://www.rdocumentation.org/packages/pheatmap/versions/1.0.10/topics/pheatmap</a>
DESeq2	<a href="#">Love et al., 2014</a>	<a href="https://bioconductor.org/packages/release/bioc/html/DESeq2.html">https://bioconductor.org/packages/release/bioc/html/DESeq2.html</a>
Ingenuity Pathway Analysis (IPA®)	<a href="#">Krämer et al., 2014</a>	<a href="https://digitalinsights.qiagen.com/products-overview/discovery-insights-portfolio/content-exploration-and-databases/qiagen-ipa/">https://digitalinsights.qiagen.com/products-overview/discovery-insights-portfolio/content-exploration-and-databases/qiagen-ipa/</a>
Cellranger® (3.0.1)	N/A	<a href="https://support.10xgenomics.com/single-cell-gene-expression/software/pipelines/latest/what-is-cell-ranger">https://support.10xgenomics.com/single-cell-gene-expression/software/pipelines/latest/what-is-cell-ranger</a>
R package: Seurat (version 3.0.2)	N/A	<a href="https://github.com/satijalab/seurat">https://github.com/satijalab/seurat</a>
singleR	<a href="#">Aran et al., 2019</a>	<a href="https://github.com/dviraran/SingleR">https://github.com/dviraran/SingleR</a>
STAR	<a href="#">Dobin et al., 2013</a>	<a href="https://github.com/alexdobin/STAR">https://github.com/alexdobin/STAR</a>
GraphPad Prism	GraphPad Software	N/A

## LEAD CONTACT AND MATERIALS AVAILABILITY

Further information and requests for resources and reagents should be directed to and will be fulfilled by the lead contact, Johannes Schlachetzki ([jschlachetzki@health.ucsd.edu](mailto:jschlachetzki@health.ucsd.edu)).

This study did not generate new unique reagents.

## EXPERIMENTAL MODEL AND SUBJECT DETAILS

### Animals

TNFtg mice (strain Tg197) were kindly provided by George Kollias (Fleming Institute, Vari, Greece) and characterized according to previous studies ([Keffer et al., 1991](#); [Süß et al., 2015](#)). These mice develop a chronic progressive form of arthritis starting at an age of 4 weeks. Arthritis in TNFtg mice is driven by constitutive overexpression of human TNF- $\alpha$  under the murine TNF- $\alpha$  promoter

due to a replacement of the regulatory 3'-UTR by the human  $\beta$ -globin gene. Expression of human TNF- $\alpha$  was reported predominantly in myeloid cells. In a previous study, we did not detect expression of human TNF- $\alpha$  in the brain of TNFtg mice (Süß et al., 2015).

Female wild-type (wt) mice were bred with male heterozygous TNFtg mice on a C57BL/6 background. Unless otherwise stated, experiments were performed with female wt and heterozygous TNFtg offspring. All mice were housed under a light-dark cycle of 12 h and had free access to food and water at the Franz Penzoldt Center (University Hospital Erlangen, Germany). At the age of 12–14 weeks, which corresponds to an advanced disease stage, mice were anaesthetized and transcardially perfused with 0.9% sodium chloride prior to tissue harvesting. For the treatment experiments with the monoclonal antibody directed against human TNF- $\alpha$ , TNFtg mice at the age of 12 weeks received two i.p. injections weekly of either IFX (10 mg/kg) or vehicle for two weeks. Mice were sacrificed one day after the last injection.

All experiments were conducted according to the National Institutes of Health and the European (2010/63/EU) guidelines for the humane treatment of animals and approved by the local government commission of animal health.

### Human Postmortem Brain Tissue

Experiments on human tissue samples were performed in accordance with the Declaration of Helsinki. Ethical approval was obtained from the local Research Ethics Committee of the University Freiburg Medical Center (reference number 10008/09). All human samples were derived from the autopsy case archive of the Institute of Neuropathology, University of Freiburg. A detailed overview of RA and control patients analyzed is shown in Table S6. Brains were transferred into 4% paraformaldehyde within less than 48h after death and fixed for at least one week. After fixation, the left frontal cortex and cerebellum were dissected and embedded in paraffin.

## METHOD DETAILS

### Murine Tissue Processing and Immunostainings

Brains of wt and TNFtg mice were removed and cut into hemispheres. Tissue was postfixed in 4% paraformaldehyde (PFA) in phosphate-buffered saline (PBS, pH 7.4) overnight and subsequently stored in 30% sucrose in 0.1 M phosphate buffer (PB, pH 7.4) until further processing. Brains were cut sagittally into 40- $\mu$ m-thick sections with a sliding microtome (Leica SM 2010R, Leica, Nussloch, Germany) on dry ice. For immunofluorescence staining of CD169, collagen IV, albumin, and fibrinogen, brain tissue harvested from both male and female mice was fixed in PFA for 5 h and cut into 20- $\mu$ m-thick sections. Sections were stored at  $-20^{\circ}\text{C}$  in cryoprotectant solution (CPS, 25% ethylene glycol, 25% glycerol in 0.1 M PB, pH 7.4) until staining.

The following primary antibodies were used for immunostainings: rat anti-CD45, 1:1,000 (IBL-3/16, Bio-Rad, Hercules, CA, USA), rat anti-CD169, 1:100 (MOMA-1, AbD Serotec, Oxford, UK), rabbit anti-ionized calcium binding adaptor molecule 1 (Iba1), 1:500 (polyclonal, Wako, Osaka, Japan), mouse anti-NeuN, 1:500 (MAB377, Merck-Millipore, Burlington, MA, USA), goat anti-gial fibrillary acidic protein (GFAP), 1:1,000 (polyclonal, Santa Cruz Biotech, Santa Cruz, CA, USA), rabbit anti-Olig2, 1:500 (polyclonal, Merck-Millipore), goat anti-collagen IV, 1:200 (polyclonal, Merck-Millipore), rabbit anti-albumin, 1:800 (polyclonal, Abcam, Cambridge, MA, USA), rabbit anti-fibrinogen, 1:500 (polyclonal, Dako, Glostrup, Denmark), rat anti-CD31, 1:200 (sc-18916, Santa Cruz Biotech) and mouse anti-claudin 5 (Cldn5), 1:300 (4C3C2, Thermo Fisher Scientific, Waltham, MA, USA).

Immunohistochemical staining was performed with every 12<sup>th</sup> section as previously described (Schlachetzki et al., 2016). Briefly, free-floating sections were rinsed in Tris-buffered saline (TBS) containing 0.05% Triton X-100 (TX100) initially and between each of the steps mentioned below. Sections were pretreated with 0.6%  $\text{H}_2\text{O}_2$  for 30 min to block endogenous peroxidase activity. For CD45 staining, sections were further submitted to antigen retrieval in citrate buffer (Dako) at  $80^{\circ}\text{C}$  for 30 min. Subsequently, sections were incubated in blocking solution consisting of 3% normal donkey serum and 3% TX100 in TBS for at least 1 h to block nonspecific antibody binding sites. Sections were kept in primary antibody solution overnight at  $4^{\circ}\text{C}$ . The next day, biotin-labeled donkey antibodies (1:300, Dianova, Hamburg, Germany) against the corresponding primary antibody species were incubated for 1 h at room temperature. After 1 h incubation in avidin-biotin peroxidase complex solution (Vectastain Elite, Vector Laboratories, Burlingame, CA, USA), final chromogenic reaction was induced with a solution of 3,3'-diaminobenzidine (DAB, 0.25 mg/ml, Vector Laboratories).

For immunofluorescence, sections were incubated in blocking solution containing 3% normal donkey serum for at least 1 h, followed by primary antibody solution overnight at  $4^{\circ}\text{C}$ . Fluorochrome-labeled donkey-derived secondary antibodies (1:500, Dianova) were incubated for 1 h. Nuclei were counterstained with DAPI. Sections were mounted and covered with ProLong Gold antifade reagent (Thermo Fisher Scientific).

### Histological Quantification

All counting procedures were carried out on blind coded slides. Immunohistochemical staining were analyzed with a light/fluorescence microscope (AxioImager M2, Zeiss, Jena, Germany) using StereoInvestigator software (MicroBrightField, Colchester, VT, USA). To quantify Iba1<sup>+</sup> cells, brain regions were assessed on at least three different sections. Regions of interest (ROI) were defined by outlining the corresponding brain region excluding the meninges. Positive cells were quantified with the Optical Fractionator tool defining a grid size of  $500 \times 500 \mu\text{m}$  and a counting frame of  $250 \times 250 \mu\text{m}$ . To obtain cell densities, cell numbers were divided by the ROI volume (ROI area  $\times$  40  $\mu\text{m}$ ). CD169<sup>+</sup> leptomeningeal macrophages were counted on at least three cortical and cerebellar sections per animal. Cell numbers were normalized to the length of meningeal lining.

To quantify the co-expression of CD45 and CD169 in Iba1<sup>+</sup> cells, ten representative multichannel images of the cortex, striatum, thalamus, hippocampus, and cerebellum derived from at least three sections were taken for each animal under a 20x objective using an inverted fluorescence microscope (Axio Observer.Z1, Zeiss) equipped with an ApoTome (Zeiss). To analyze the co-expression of Iba1, NeuN, Olig2 and GFAP in CD45<sup>+</sup> and CD169<sup>+</sup> cells, ten representative images of the thalamus were taken for each TNFtg mouse. Co-expression analysis was performed using Zen Blue software (Zeiss).

To determine the ratio of CD31<sup>+</sup> blood vessels positive for claudin 5 (Cldn5) and to assess the extravascular leakage of albumin and fibrinogen in different brain regions, representative images were taken on a confocal laser-scanning microscope (LSM 780, Zeiss) and analyzed using the colocalization tool provided by the ZEN Black software (Zeiss). For albumin- and fibrinogen co-staining with collagen IV, 4 z stacks with steps of 0.75  $\mu\text{m}$  in z direction and 3,440  $\times$  3,440 pixels in xy-resolution were taken from cortex and cerebellum using a 20x objective. For CD31 and Cldn5, at least 3 z stacks with steps of 1.0  $\mu\text{m}$  in z-direction and a xy-resolution of 1,024  $\times$  1,024 pixels were taken from each brain region under a 63x objective. Colocalization was determined for at least 10 blood vessels per animal and region. For albumin- and fibrinogen co-staining with collagen IV, 4 images per region and animal were taken under a 20x objective.

### Evans Blue Assay

At an age of 14 weeks, male and female wt and TNFtg mice received an intravenous injection of 25 mg/kg Evans Blue dissolved in PBS. After 4 h, brain tissue was removed and dissected into the respective brain regions. Lung tissue was dissected from  $n = 2$  mice per group as a positive control. Dissected tissue was weighed and incubated with 5  $\mu\text{l}$  formamide per mg tissue overnight at 60°C. Adsorption at a wavelength of 620 nm was measured using an ELISA reader and concentrations of Evans Blue were inferred with the help of a calibration curve created from adsorption values of six samples with predefined Evans Blue concentrations.

### Isolation and Immunophenotyping of CNS Myeloid Cells

For the isolation of myeloid cells from mouse brain or dissected cortex, male and female wt and TNFtg mice were anesthetized and perfused intracardially with ice cold PBS. Brains were dissected and mechanically homogenized in ice-cold dissection medium consisting of Hank's Balanced Salt Solution (HBSS), HEPES buffer and 0.5% glucose. Resulting cell suspensions were centrifuged and resuspended in 37% Percoll (Sigma-Aldrich, St. Louis, MO, USA). Next, cells were centrifuged for 30 min at 800  $\times$  g and 4°C. Following additional washing and centrifugation steps, samples were resuspended in staining buffer (4% fetal bovine serum in PBS) and were stored on ice during staining and analysis. Fc $\gamma$  receptors were blocked for 15 min (TruStain fcX, BioLegend, San Diego, California, USA).

For flow cytometry analyses, surface antigens on cells were stained for 30 min at 4°C with the following antibodies: anti-CD11b (M1/70), anti-CD45 (30-F11), anti-MHC-II (M5/114.15.2), anti-Ly6C (HK1.4), and anti-Ly6G (1A8, all from BioLegend). Additionally, live/dead-staining was performed using eBioscience eFluor 780 Fixable Viability Dye (eBioscience, San Diego, CA, USA). Cellular fluorescence was assessed with CytoFLEX (Beckman Coulter, Brea, CA, USA) and data were analyzed with FlowJo software (version 10, TreeStar Inc., Ashland, OR, USA).

### RNA Isolation and qPCR

Brains of wt ( $n = 4$ ) and TNFtg mice ( $n = 4$ ) were removed and cut into hemispheres. Cerebellum, hippocampus, thalamus, striatum, and cortex from both hemispheres were immediately dissected on ice and stored at  $-80^\circ\text{C}$ . Dissected brain regions from the left hemisphere were assigned for RNA sequencing, whereas qPCR analysis was performed with right hemispheric regions.

Dissected right hemispheric regions were mechanically homogenized in QIAzol reagent (QIAGEN, Hilden, Germany) and RNA was isolated using RNeasy Plus Mini Kit (QIAGEN). The attained concentration of RNA was determined using the NanoDrop spectrophotometric system (Peqlab, Erlangen, Germany). Samples with an RNA concentration below 25 ng/ $\mu\text{l}$  were not used for further analysis ( $n = 1$  TNFtg for striatum, thalamus, and cerebellum;  $n = 2$  TNFtg for cortex). RNA of remaining samples was transcribed into 125 ng of cDNA with Random Primers and GoScript Reverse Transcription System (Promega, Fitchburg, WI, USA).

To compare mRNA levels in different brain regions of wt and TNFtg mice, qPCR was carried out as described previously (Süß et al., 2015). Primers used in this study are listed in Table S1. Relative mRNA levels were calculated by the  $\Delta\Delta\text{Ct}$  method and normalized to cerebellar levels of wt animals.

### Region-Specific Bulk RNA Sequencing

Poly(A) selection of RNA was performed as previously described (Gosselin et al., 2014). Briefly, RNA samples were incubated with Oligo d(T) Magnetic Beads (NEB, Ipswich, MA) and poly(A) enriched RNA was collected. To fragment poly(A) RNA, samples were incubated at 94°C for 9 min on beads. First-strand synthesis and second-strand synthesis as well as blunting, A-tailing, and adaptor ligation was done using barcoded adapters (NextFlex, Bio Scientific) as previously described (Gosselin et al., 2014). Libraries were PCR-amplified for 12-15 cycles and size selected for fragments (200-350 bp) by gel extraction (10% TBE gels, Life Technologies EC62752BOX). RNA-seq libraries were single-end sequenced for 51 cycles on an Illumina HiSeq 2500 (Illumina, San Diego, CA) according to manufacturer's instruction.

### Differential Gene Expression and Variability Analysis

FASTQ files demultiplexed by Illumina *bcl2fastqs* from HiSeq4000 sequencing experiments were mapped to the UCSC genome build mm10. STAR with default parameters was used to map RNA-seq experiments (Dobin et al., 2013). The “analyzeRepeats” function of HOMER was used to quantify the gene expression raw counts with the parameters “-raw -count exons -strand both -condense-Genes” and a table of reads per kilobase per million mapped reads (RPKM) values using “-rpkm -normMatrix 1e7 -count exons -strand both -condenseGenes” (Heinz et al., 2010). Raw counts within each gene body were used as input for DESeq2. Significance was assessed at a false discovery rate (FDR) of 0.05 using the Benjamini-Hochberg method and an effect size cutoff of 2-fold change in expression. For heatmaps and principal component analysis (PCA), RPKM of the 497 genes differentially expressed in at least one brain region were determined. Average RPKM values were calculated for each group. Heatmaps were based on Canberra distance matrices and Ward’s minimum variance method for hierarchical clustering of groups with the pheatmap package in R. Gene ontology (GO) enrichment analysis was done using Metascape (<http://metascape.org>) (Tripathi et al., 2015).

Regional log<sub>2</sub> fold changes between TNFtg and wt mice of the 127 genes commonly upregulated in the cortex, striatum, and thalamus of TNFtg mice were analyzed through Ingenuity Pathway Analysis (IPA®) from QIAGEN® (Krämer et al., 2014). Comparative analysis of all five brain regions was performed and on canonical pathways, upstream regulators, and diseases and functions were inferred after filtering for “mouse” as species and “nervous system” as the tissue of interest.

### Single Cell RNA Sequencing

Brain myeloid cells were isolated as described previously (Gosselin et al., 2014, 2017). Briefly, the cortex of 14-week old female wt and TNFtg (n = 2 per experimental group) were dissected and homogenized by gentle mechanical dissociation at 4°C. Myeloid cells were enriched by Percoll gradient, washed, and then stained for DAPI and with anti-CD11b and anti-CD45 antibody. Life CD11b<sup>+</sup>CD45<sup>+</sup>DAPI<sup>-</sup> cells (containing CD45<sup>hi</sup> and CD45<sup>low/int</sup> cells) were sorted into PBS containing 0.04% BSA. Cells were centrifuged and resuspended to an adjusted concentration of 1,000 cells/μl. Equal numbers of cells from two mice per group were pooled. Using the 10X GemCode technology, single cells were captured with barcoded beads in a droplet emulsion for the RT reaction (10X Genomics®). Libraries were prepared following the standard protocol of 10X Single Cell 3’ v3.0 and sequenced on the Hi-Seq 4000 (Illumina). Cellranger® (3.0.1) from 10X Genomics® was used for mapping and gene expression quantification on mm10 reference genome. We used the R package Seurat (version 3.0.2) to perform quality control and clustering analysis. Cells expressing < 200 or > 4000 genes were filtered out to exclude non-cells or cell aggregates. We filtered out cells that contained a percentage of mitochondrial genes > 15%. Unique molecular identifiers which barcode each individual mRNA molecule within a cell during reverse transcription were used to identify highly variable genes and to calculate the principal component based on these genes. The first 18 principle components determined by the Jackstraw procedure were used for the tSNE dimensionality reduction and clustering was performed using the shared nearest neighbor (SNN) modularity optimization. For unbiased cell type recognition, we used singleR (Aran et al., 2019).

### Immunohistochemistry of Human Postmortem Tissue

To determine regional IBA1<sup>+</sup> and P2RY12<sup>+</sup> cell densities, IHC was performed on 3 μm thick sections from human postmortem brain specimen (frontal cortex and cerebellum). Sections were deparaffinized and heated at 92°C, at pH 6 for 40 min for antigen retrieval, followed by incubation with the respective primary antibodies for 30 min at room temperature: rabbit anti-IBA-1, 1:1,000 (Abcam, clone EPR 16588), and rabbit anti-P2RY12, 1:1,500 (Sigma-Aldrich, polyclonal). After washing, secondary goat anti-rabbit antibodies (Southern Biotech), 1:200, were added for 1 h at room temperature. Antigens were visualized by 3,3’-Diaminobenzidine (DAB). Nuclei were counterstained with hematoxylin. For both stainings, 10 representative cortical and cerebellar images were taken using an Olympus BX61 brightfield microscope (Olympus) with a 10x objective. While cortical images were randomly distributed throughout the six cortical layers, cerebellar images consisted of five images of the cortex cerebelli and five images of the cerebellar white matter. Images were analyzed using ImageJ.

### QUANTIFICATION AND STATISTICAL ANALYSIS

All data are displayed as means ± SEM. Statistical analysis was performed using unpaired Student’s t test to compare two groups and 2-way ANOVA followed by Bonferroni’s multiple-testing correction to compare the effect of genotype or IFX treatment in different brain regions. Significance was set at p < 0.05.

### DATA AND CODE AVAILABILITY

The accession number for the RNA-seq data reported in this paper is: E-MTAB-7279. The accession number for the raw data and processed data generated by single cell RNA-seq is GEO: GSE145708.

**Cell Reports, Volume 30**

**Supplemental Information**

**Chronic Peripheral Inflammation Causes**

**a Region-Specific Myeloid Response**

**in the Central Nervous System**

**Patrick Süß, Alana Hoffmann, Tobias Rothe, Zhengyu Ouyang, Wolfgang Baum, Ori Staszewski, Georg Schett, Marco Prinz, Gerhard Krönke, Christopher K. Glass, Jürgen Winkler, and Johannes C.M. Schlachetzki**

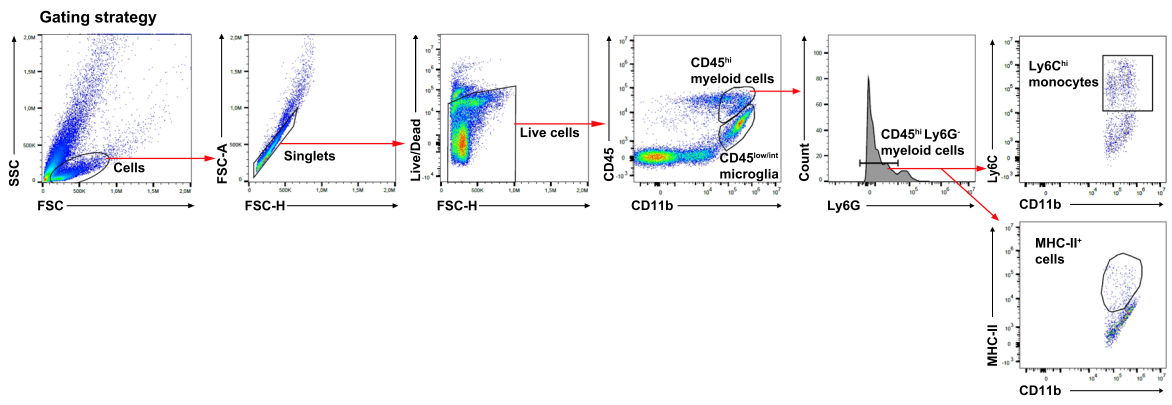


Figure S1

**Figure S1. Gating strategy for flow cytometry experiments.** Related to Figures 1,2, and 6. Cells were gated on CD11b and CD45 for the separation of CD11b<sup>+</sup>CD45<sup>low/int</sup> homeostatic microglia from CD11b<sup>+</sup>CD45<sup>hi</sup> myeloid cells. CD11b<sup>+</sup>CD45<sup>hi</sup> myeloid cells were further gated on Ly6G<sup>-</sup> to exclude granulocytes and characterized regarding Ly6C and MHC-II expression levels.

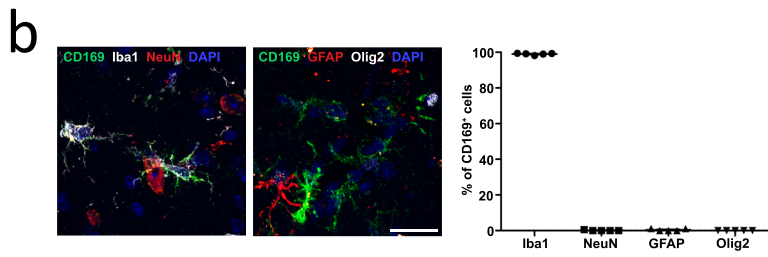
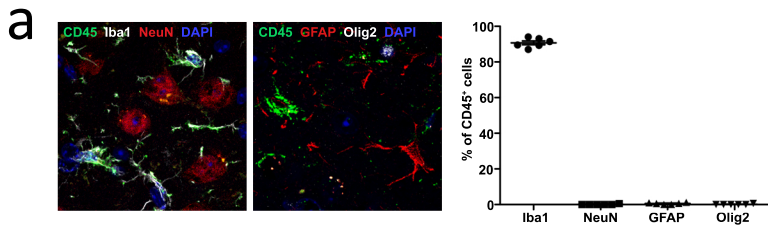
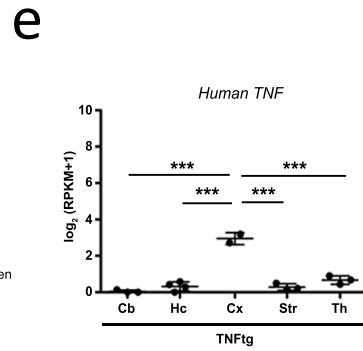
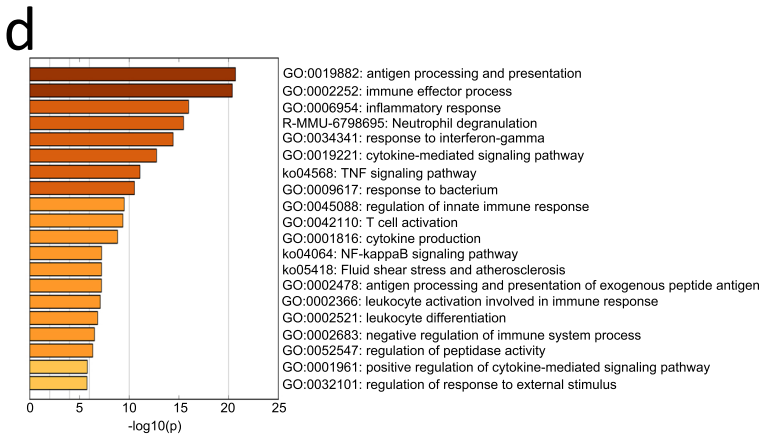
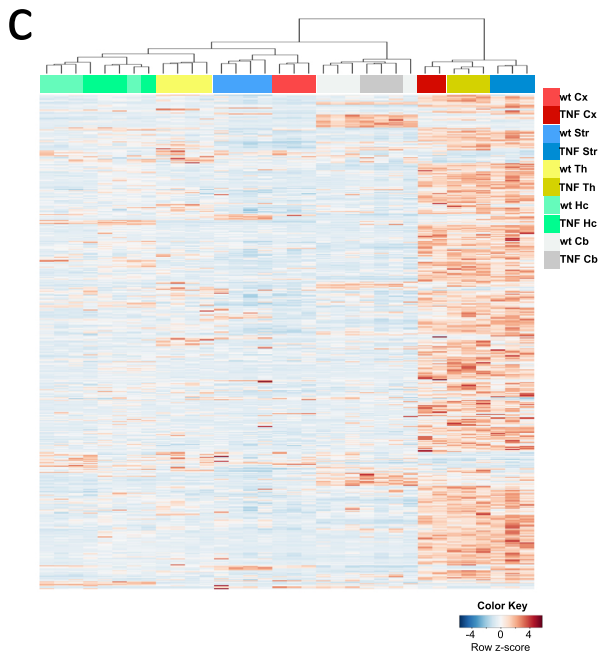
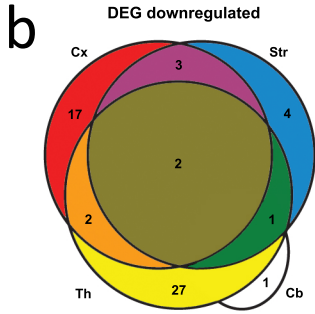
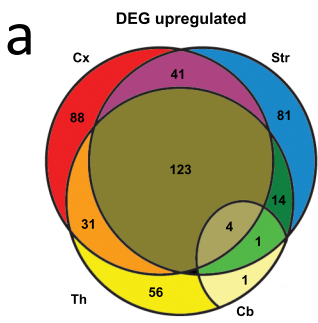


Figure S2

**Figure S2. Specific expression of CD45 and CD169 in myeloid cells.** Related to Figures 2 and 6. (a) Expression rates of Iba1, NeuN, GFAP, and Olig2 in CD45<sup>+</sup> cells. (b) Expression rates of Iba1, NeuN, GFAP, and Olig2 in CD169<sup>+</sup> cells. Scale bars: 20  $\mu$ m. Data are derived from the thalamus of TNFtg mice and representative of n=6 (a) or n=5 (b) animals. Data are shown as mean  $\pm$  S.E.M.



FigureS3

**Figure S3. Regional inflammatory response in the brain of TNFtg mice revealed by bulk RNA-seq.** Related to Figure 3. (a) Venn diagram showing the regional overlap of upregulated genes in TNFtg mice. (b) Venn diagram showing the regional overlap of downregulated genes in TNFtg mice. (c) Heat map showing hierarchical clustering of all individual samples based on n=497 genes differentially expressed in brain regions of TNFtg mice compared to wt mice. (d) Heat map indicating the most significantly enriched GO-terms in n=127 genes commonly upregulated in the cortex (Cx), striatum (Str), and thalamus (Th) of TNFtg mice. (e) Expression levels of human TNF in the Cx, Str, Th, Hc and Cb of TNFtg mice. FASTQ files were mapped onto UCSC genome build hg38. Data are depicted as mean  $\pm$  S.E.M., \*\*\* $p < 0.001$ .

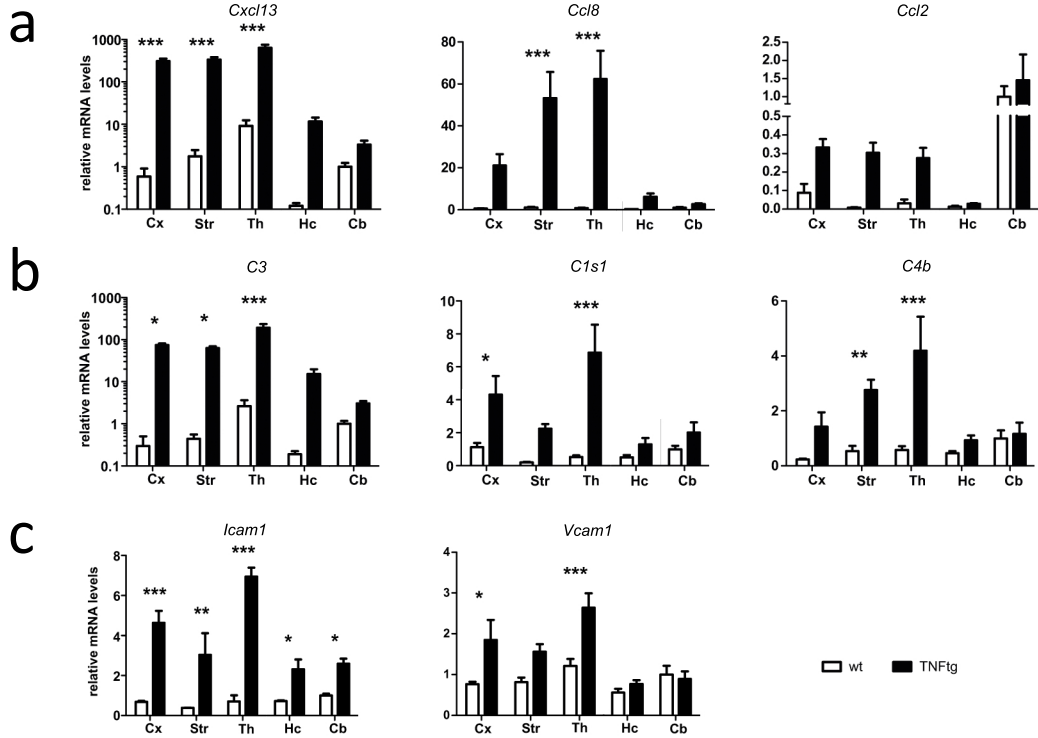


Figure S4

**Figure S4. Regional transcriptional inflammatory response in the brain of TNFtg mice confirmed by qPCR.** Related to Figure 3. (a) Transcriptional levels of the chemokines *Cxcl13*, *Ccl8*, and *Ccl2* in brain regions of wt and TNFtg mice. (b) Regional transcriptional levels of genes encoding the complement factors *C3*, *C1s1*, and *C4b*. (c) Regional mRNA levels of *Icam1* and *Vcam1* in wt and TNFtg mice. Data are representative of n=4 animals per genotype and region from two independent experiments and are presented as mean  $\pm$  S.E.M. Analysis was performed using two-way ANOVA followed by Bonferroni's post-hoc test, \*p<0.05, \*\*p<0.01, \*\*\*p<0.001.

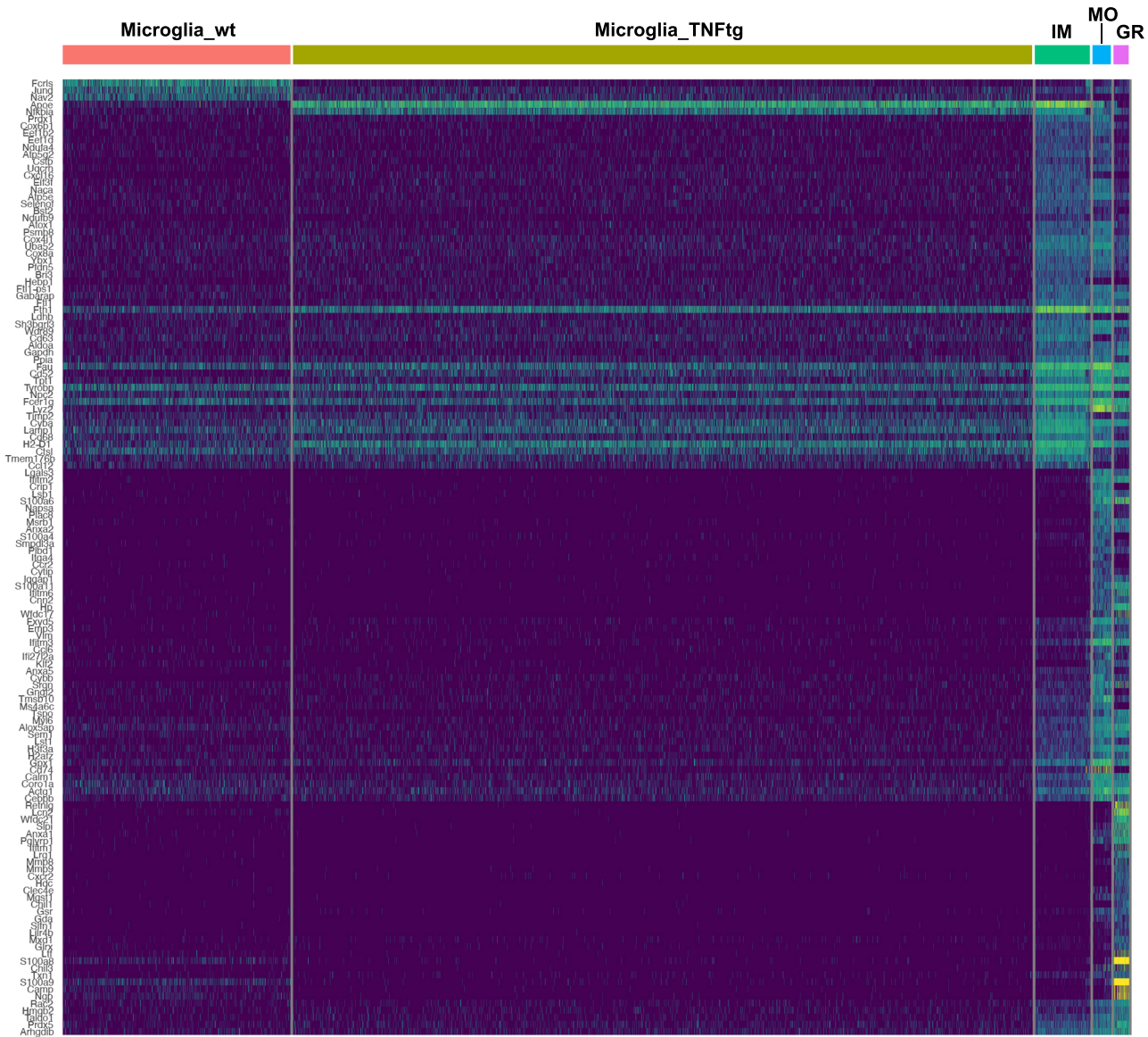


Figure S5

**Figure S5. Heat map of differentially expressed genes in myeloid cell clusters.**

Related to Figure 4. IM: Inflammatory macrophages, MO: Monocytes, GR: Granulocytes.

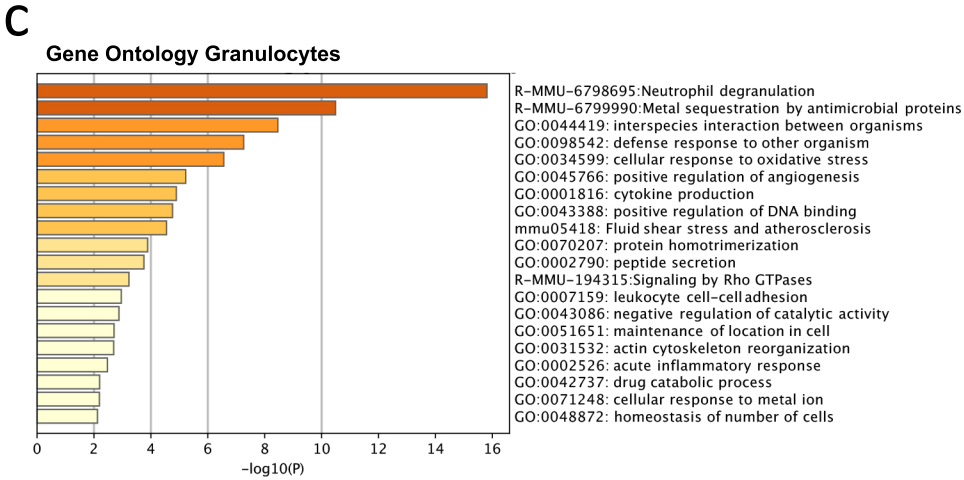
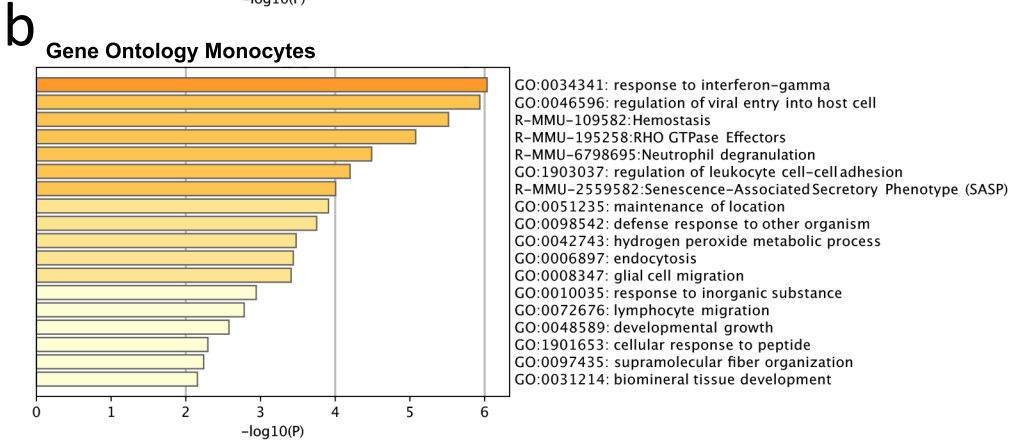
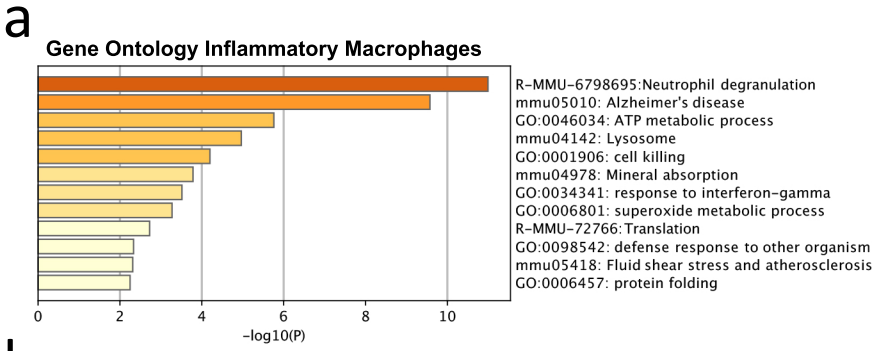
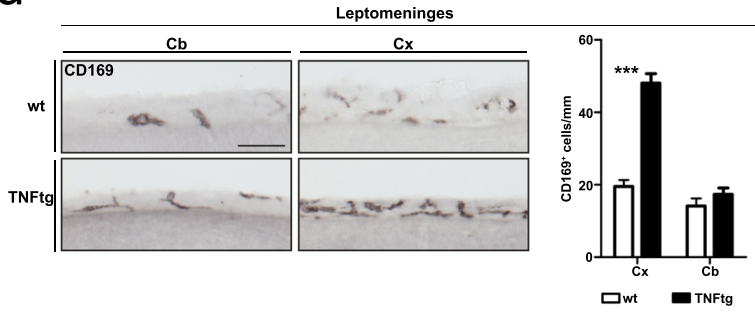
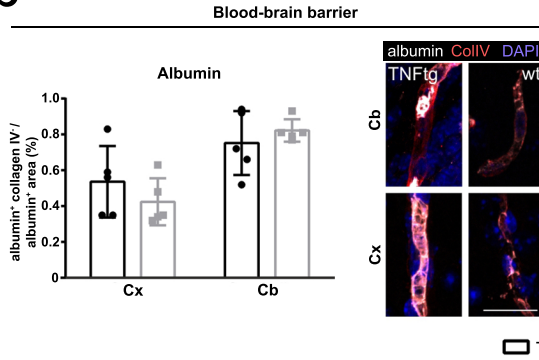
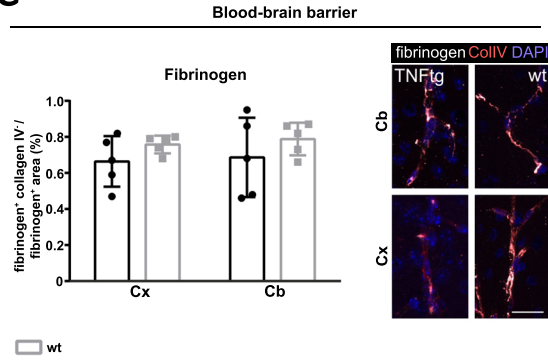
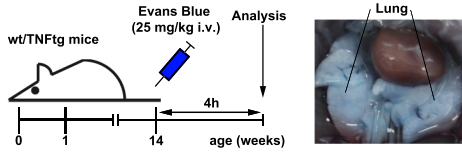


Figure S6

**Figure S6. Gene ontology of myeloid clusters identified by scRNA-seq.** Related to Figure 4. (a) Enriched Gene Ontology (GO) terms in the inflammatory macrophage cluster (cluster 2). (b) Enriched GO terms in the cluster of monocytes. (c) Enriched GO terms in granulocytes.

**a****b****c****d****Figure S7**

**Figure S7. Analysis of CNS borders in TNFtg mice.** Related to Figure 5. (a) Densities of CD169<sup>+</sup> leptomeningeal macrophages in vicinity to the cortex (Cx) and cerebellum (Cb) of wt (n=5) and TNFtg mice (n=6). Scale bar: 50  $\mu$ m. (b, c) Intensity-adjusted fraction of albumin (b)- and fibrinogen (c)-positive area not overlapping with collagen IV (ColIV) staining in the cortex (Cx) and cerebellum (Cb) of wt and TNFtg mice (n=5 per group). Scale bars: 20  $\mu$ m. (d) Experimental scheme of Evans Blue injection and in-situ image of the lung as a positive control for Evans Blue uptake. Data are shown as mean  $\pm$  S.E.M. Analysis was performed using two-way ANOVA followed by Bonferroni's post-hoc test, \*\*\*p<0.001.